Phys Chem Minerals (2004) 31: 1–20
DOI 10.1007/s00269-004-0400-4

ORIGINAL PAPER

F. Hatert · G. J. Long · D. Hautot · A.-M. Fransolet
J. Delwiche · M. J. Hubin-Franskin · F. Grandjean

A structural, magnetic, and Mössbauer spectral study of several Na–Mn–Fe-bearing alluaudites

Received: 20 August 2003 / Accepted: 11 April 2004

Abstract The synthesis and the chemical, structural, magnetic, and Mössbauer spectral characterization of three synthetic alluaudites, $Na_2Mn_2Fe(PO_4)_3$, $NaMnFe_2(PO_4)_3$ and $Na_2MnFe^{II}Fe^{III}(PO_4)_3$, and a natural sample with the nominal composition of $NaMnFe_2(PO_4)_3$, collected in the Buranga pegmatite, Rwanda, are reported. All four compounds have the expected alluaudite monoclinic $C2/c$ structure with the general formula $[A(2)A(2)'][A(1)A(1)'A(1)_2'']M(1)M(2)_2(PO_4)_3$ in which manganese(II) is on the $M(1)$ site and manganese(II), iron(III) and, in some cases, iron(II) on the $M(2)$ site. The X-ray structure of $Na_2Mn_2Fe(PO_4)_3$ also indicates a partially disordered distribution of Na^1 and Mn^{II} on the $M(1)$ and $A(1)$ crystallographic sites. All four compounds are paramagnetic above 40 K and antiferromagnetically ordered below. Above 40 K the effective magnetic moments of $NaMnFe_2(PO_4)_3$ and $Na_2MnFe^{II}Fe^{III}(PO_4)_3$ are those expected of high-spin manganese(II) and iron(III) with the $^6A_{1g}$ electronic ground state and high-spin iron(II) with the $^5T_{2g}$ electronic ground state. In contrast, the effective magnetic moment of $Na_2Mn_2Fe(PO_4)_3$ is lower than expected as a result of enhanced antiferromagnetic exchange coupling by the manganese(II) on the $M(2)$ site. The Mössbauer spectra of all four compounds have been measured from 4.2 to 295 K and have been found to be magnetically ordered below 40 K for $Na_2Mn_2Fe(PO_4)_3$ and ~35 K for the remaining compounds. The Mössbauer spectra of $Na_2Mn_2Fe(PO_4)_3$ exhibit the two expected iron(III) quadrupole doublets and/or magnetic sextets expected for a random distribution of manganese(II) and iron(III) ions on the $M(2)$ site. Further, the Mössbauer spectra of $Na_2MnFe^{II}Fe^{III}(PO_4)_3$ exhibit the two iron(II) and two iron(III) quadrupole doublets and/or magnetic sextets expected for a random distribution of iron(II) and iron(III) on the $M(2)$ site. Surprisingly, the synthetic and natural samples of $NaMnFe_2(PO_4)_3$ have 19 and 10% of iron(II) on the $M(2)$ site; apparently the presence of some iron(II) stabilizes the alluaudite structure through the reduction of iron(III)–iron(III) repulsion. The temperature dependence of the iron(II) quadrupole splitting yields a 440 to 600 cm^{-1} low-symmetry component to the octahedral crystal field splitting at the $M(2)$ site. The iron(II) and iron(III) hyperfine fields observed at 4.2 K are consistent with the presence of antiferromagnetic ordering at low temperatures in all four compounds.

Keywords Alluaudites · Iron phosphate · Magnetic interactions · Mössbauer spectroscopy

F. Hatert · A.-M. Fransolet (✉)
Laboratory of Mineralogy,
University of Liège, B18,
4000 Sart-Tilman, Belgium

G. J. Long (✉) · D. Hautot
Department of Chemistry,
University of Missouri-Rolla,
Rolla, Missouri 65409-0010, USA

J. Delwiche · M. J. Hubin-Franskin
Institute of Chemistry, B6,
University of Liège,
4000 Sart-Tilman, Belgium

F. Grandjean (✉)
Institute of Physics, B5,
University of Liège,
4000 Sart-Tilman, Belgium

[1] Unfortunately, an incorrect equation was used in our earlier work (Hatert et al. 2003; Hermann et al. 2002), to fit the temperature dependence of the iron(II) quadrupole splittings. Equation (1) is the correct equation and the correct values have been used herein for comparison.

Introduction

Thealluaudite structure provides an excellent template within which to study the magnetic interaction in natural and synthetic minerals. The alluaudite minerals and their structural porperties have been known for many years and have been summarized recently by Hatert et al. (2000).

The crystal structure of a natural alluaudite sample from Buranga, Rwanda, was reported by Moore (1971), who found that the mineral was monoclinic with the $C2/$

2 6 9 _ 0 4 0 0 B | Dispatch: 15.6.2004 | Journal: Phys Chem Minerals | No. of pages: 20
Journal number | Manuscript number | Author's disk received ☑ | Used ☑ | Corrupted ☐ | Mismatch ☐ | Keyed ☐

c space group and the structural formula, $X(2)X(1)M(1)M(2)_2(PO_4)_3$, with four formula units per unit cell. The actual composition of alluaudite minerals may vary between $Na_2MnFe_2(PO_4)_3$ and $\square NaMnFe_2(PO_4)_3$, where the first composition is a mixed valent mineral with equal amounts of iron(II) and iron(III) and the second contains only iron(III). In the second composition $\square$ represents a lattice vacancy.

Over the past 20 years a variety of synthetic alluaudite-like compounds have been reported; see Hatert et al. (2000) for a brief summary of this work. The study of these new alluaudite-like structures reveals more structural complexity than that reported by Moore (1971), a complexity which results from cationic sites not reported earlier. This complexity is best represented as $[A(2)A(2)'][A(1)A(1)'A(1)_2'']M(1)M(2)_2(PO_4)_3$, a formulation in which the crystallographic *A* sites may be either empty or partially filled and the *M* sites must be filled. Thus, in $\square NaCdIn_2(PO_4)_3$ the *A*(1) site is filled with Na^I and the remaining *A* sites are empty (Antenucci et al. 1993) whereas in $\square NaMnFe_2(PO_4)_3$ both the *A*(1) and *A*(2)'sites contain Na^I (Hatert et al. 2000). In order to avoid confusion, in this paper we will use the more complex formulation to describe the crystallographic sites in the compounds under study.

Alluaudite has an open structural framework with *A*(1) channels which may contain cations, such as Na^I, and *A*(2)' channels which may either contain a cation or be empty. Of more importance to the study of the magnetic properties of the alluaudite-like minerals are the chains containing the *M*(1) and *M*(2) sites with distorted octahedral coordination environments, chains which are bridged by the phosphate anions. These chains, which typically contain divalent and/or trivalent metal cations, are made up of edge-sharing octahedra in which pairs of *M*(2) sites are separated by single *M*(1) sites. These chains, the details of which are shown in Fig. 1, are oriented parallel to the {101} plane, are ''staggered or kinked'' along the *c* axis, and are well separated by the phosphate groups along the *b* axis. Thus, by changing the cations in the *M*(1) and *M*(2) sites, and by using either diamagnetic or paramagnetic cations, it is possible to modulate the magnetic interactions along the chain.

The flexibility of the alluaudite structure will, no doubt, permit the use of alluaudite-type compounds for practical applications, such as corrosion inhibition, passivation of metal surfaces, and catalysis (Korzenski et al. 1998). Due to the presence of channels parallel to the *c* axis, alluaudite-type compounds exhibit electronic and/or ionic conductivity properties, as has been shown by Warner et al. (1994), Daidouh et al. (2002), and Durio et al. (2002). The possibility of inserting variable amounts of lithium into the channels of the alluaudite structure also makes the $(Na_{1-x}Li_x)MnFe^{3+}{}_2(PO_4)_3$ compounds of value as potential battery materials (Hatert et al. 2000; Richardson 2003).

Although there have been many structural studies of alluaudites, there have been relatively few studies of the magnetic properties of alluaudite-like compounds. Indeed, there are only three magnetic studies of which we are aware. In the first, Korzenski et al. (1998) reported in detail upon the structural and magnetic properties of mixed-valent $NaFe_{3.67}(PO_4)_3$, an alluaudite-like compound which is antiferromagnetically ordered below ~30 K. In the second, Chouaibi et al. (2001) studied alluaudite-like $Ag_2FeMn_2(PO_4)_3$ and reported the presence of weak ferromagnetism below 19 K, ferromagnetism which results from a canting of antiferromagnetically coupled spins. In the third, Durio et al. (2002) studied the $Na_2M_3(PO_4)_3$ alluaudites compounds with M_3 equal to FeMnCd, $InMn_2$, $GaMn_2$, and $GaCd_2$. The first three compounds are found to exhibit weak antiferromagnetic behavior below 18, 9, and 10 K, respectively, with a ''weak ferromagnetic transition at low temperature.''

The purpose of this paper is to report the electronic and magnetic properties of three synthetic alluaudite-like compounds and one natural alluaudite. Specifically, we report herein on the synthesis, and on the structural,

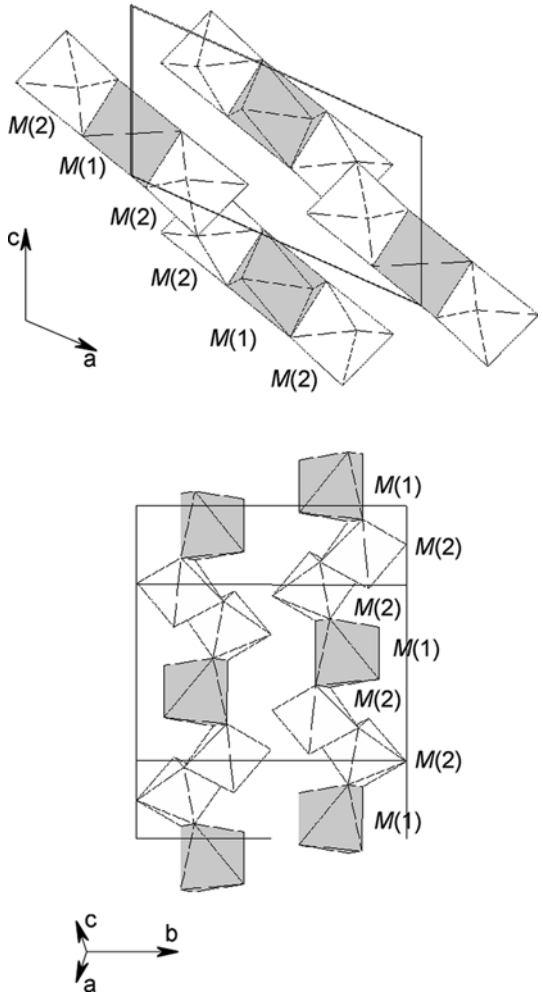

Fig. 1 A schematic representation of the chains containing the *M*(1), *gray*, and *M*(2), *white*, cationic sites in the alluaudite crystal structure

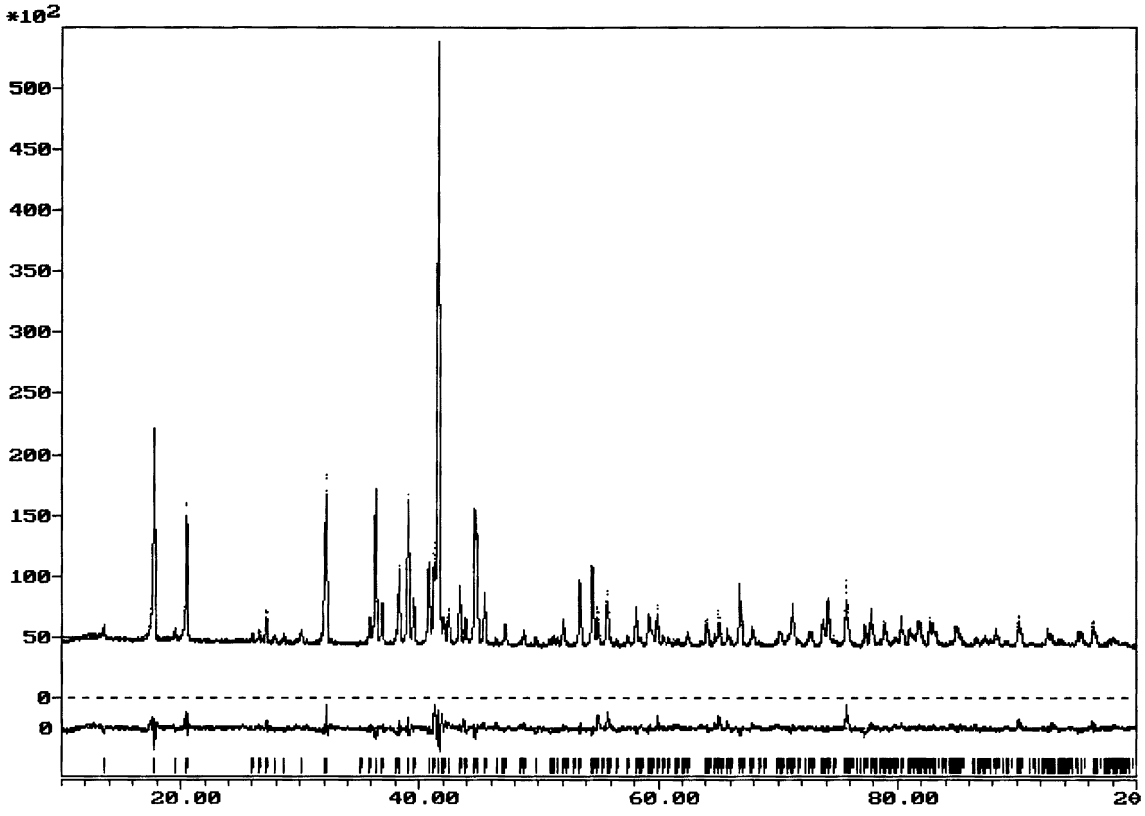

Fig. 2 The observed (*dots*), calculated (*solid line*), and difference X-ray powder diffraction patterns of $Na_2Mn_2Fe(PO_4)_3$ #1, obtained from a Rietveld refinement. The *vertical markers* indicate the positions calculated for the Fe$K\alpha_1$ and Fe$K\alpha_2$ Bragg reflections

magnetic, and Mössbauer spectral characterization of synthetic $Na_2Mn_2Fe(PO_4)_3$ #1, synthetic $NaMnFe_2(PO_4)_3$ #2, natural $NaMnFe_2(PO_4)_3$ #3, collected in the Buranga pegmatite, Rwanda (Fransolet 1975), and synthetic $Na_2MnFe^{II}Fe^{III}(PO_4)_3$ #4.

Experimental

Synthesis

$Na_2Mn_2Fe(PO_4)_3$ #1 and $NaMnFe_2(PO_4)_3$ #2 were synthesized by a solid-state reaction carried out in air. Stoichiometric quantities of $NaHCO_3$, MnO, $FeSO_4 \cdot 7H_2O$, and $NH_4H_2PO_4$ were dissolved in concentrated nitric acid, and the resulting solution was evaporated to dryness. The dry residue was progressively heated in a platinum crucible to 850 °C for #1 or 975 °C for #2, and subsequently maintained at these temperatures for 17 h. The synthesis temperatures were chosen in order to obtain high-purity alluaudites. After heating, the compounds were quenched in air.

$Na_2MnFe^{II}Fe^{III}(PO_4)_3$ #4 was synthesized under hydrothermal conditions. The starting material was prepared by mixing $NaH_2PO_4 \cdot H_2O$, MnO, FeO, and Fe_2O_3 in the appropriate proportions. An H_3PO_4 solution was added in order to achieve stoichiometry, and the mixture was homogenized in a mortar after evaporation. About 25 mg of the resulting residue was sealed into a gold tube with an outer diameter of 2 mm and a length of 25 mm, containing 5 μl of distilled water. The preparation was carried out with a conventional hydrothermal apparatus with a horizontally oriented Tuttle-type pressure vessel (Tuttle 1949) maintained at a temperature of 700 °C and a pressure of 0.35 GPa. After 21 days, the sample, still in the gold tube in the autoclave, was quenched to room temperature in a stream of cold air.

X-ray diffraction

X-ray powder diffraction patterns were recorded on a Philps PW-3710 diffractometer by using FeK_α radiation at a wavelength of 1.9373 Å. The unit-cell parameters were calculated with the least-squares refinement program LCLSQ 8.4 (Burnham 1991) from the *d* spacings callibrated with $Pb(NO_3)_2$ as an internal standard. These unit-cell parameters and the atomic positions reported for synthetic $Na_2Mn_2Fe(PO_4)_3$ #2, (Hatert et al. 2000), served as the starting parameters for the Rietveld refinement of $Na_2Mn_2Fe(PO_4)_3$ #1, refinements which were performed with the DBWS-9807 program developed by Young et al. (1998). The thermal *B* factors were fixed to values similar to those obtained by Hatert et al. (2000). The investigated 2θ range extended from 10 to 100°, the step width was 0.02°, and the step time was 15 s. The total number of refined parameters was 51, with 501 observed reflections; the final Rietveld plot is shown in Fig. 2.

Chemical analyses

The wet chemical analyses (Table 1) were performed on 100 to 300 mg of sample which had been carefully selected under a binocular microscope and checked for purity by X-ray diffraction. Atomic absorption spectrophotometry was used to determine the Al, Fe, Mn, Mg, Ca, Na, K, and Li content, whereas the P content was measured by colorimetry. The Ungethüm method (Ungethüm 1965) was used for the determination of Fe^{II}, and the amount of H_2O was determined by the Penfield method.

Microprobe analyses (Table 1) were obtained on a CAMECA SX50 instrument with an accelerating voltage of 15 kV and a probe current of 20 nA. A Kabira graftonite standard (Fransolet 1975) was used for the Mn, Fe, and P determinations, and oligoclase was used for the Na determination.

Magnetic measurements

The magnetic measurements were obtained at 4 T with between 28 and 56 mg of powdered sample using an Oxford Instruments MagLab 9 vibrating sample magnetometer which was calibrated with nickel at 295 K and 0.6 T by using a magnetization of 54.88936 emu/g^{-1} for nickel. The molar magnetic susceptibilities were corrected for diamagnetic susceptibility using Pascal's constants. The magnetic moments are estimated to have an absolute accuracy of ± 0.05 μ_B and a relative accuracy between compounds studied herein and for their temperature dependence of ± 0.02 μ_B.

Table 1 Chemical analyses, in wt%, of the natural and synthetic alluaudites

	#1[a]	#2[a]	#2[b]	#3[a]	#4[b]
P_2O_5	44.44	44.17	44.63	43.85	43.09
Al_2O_3	–	–	–	1.35	–
Fe_2O_3	16.36	29.24	28.25	27.64	15.69
FeO	0.00	3.34	3.13	1.56	15.53
MnO	27.4	17.12	19.85	17.27	15.05
MgO	–	–	–	0.49	–
CaO	–	–	–	1.33	–
Na_2O	12.28	5.92	5.55	4.80	11.62
K_2O	–	–	–	0.01	–
Li_2O	–	–	–	0.00	–
H_2O	–	–	–	1.62	–
Total	100.48	99.79	101.41	99.92	100.98
Number of cations[c]					
P^{5+}	3.058	3.001	3.000	2.987	3.000
Al^{3+}	–	–	–	0.128	–
Fe^{3+}	1.001	1.766	1.688	1.674	0.971
Fe^{2+}	0.000	0.224	0.208	0.105	1.068
Mn^{2+}	1.886	1.164	1.335	1.177	1.048
Mg^{2+}	–	–	–	0.059	–
Ca^{2+}	–	–	–	0.115	–
Na^{+}	1.935	0.921	0.854	0.749	1.853
K^{+}	–	–	–	0.001	–
Li^{+}	–	–	–	0.000	–
H_2O	–	–	–	0.435	–

[a] Wet chemical analyses by J.-M. Speetjens
[b] Electron macroprobe analyses by J. Wauthier. The number of analyses was six for compound #2 and four for compound #4
[c] Cation numbers were calculated on the basis of three P (microprobe analyses) or 12 oxygens (wet chemical analyses) per formula unit. FeO and Fe_2O_3 values, determined by microprobe analyses, were calculated in order to sum to 24 positive charges.

Mössbauer spectral measurements

The iron-57 Mössbauer spectra were measured between 4.2 and 295 K on a constant acceleration spectrometer which utilized a rhodium matrix cobalt-57 source and was calibrated at room temperature with α-iron foil. The studies were carried out in a Janis Supervaritemp cryostat and the sample temperature was regulated at ± 0.1 K. The spectra were fitted as discussed below. The absorber thicknesses were approximately 50, 67, 52, and 40 mg cm^{-2}, for compounds #1–4 respectively, and the same absorber was used at all temperatures in order to maintain a constant source-absorber-detector geometry during the measurements. Because of the use of the same absorber above and below the magnetic ordering temperature, the absorber thickess was idealized for the more expensive low-temperature measurements. As a consequence, the absorber thickness is larger than ideal for the higher temperature measurements of the paramagnetic spectra. In order to ensure that saturation effects did not influence the spectral analysis of the paramagnetic spectra, the Mössbauer spectra of sample #2 were measured at 85 K with absorber thicknesses of ~33 and 17 mg cm^{-2} as well as at 80 K with a thickness of 67 mg cm^{-2}. The results of this analysis led to an iron(II) content of 17 ± 2 vol% for the thin absorbers and 19 ± 1 vol% for the thick absorber. Thus, we conclude that saturation effects, if any, are within the quoted relative and absolute accuracies. The estimated relative accuracies are approximately ± 0.005 mm s^{-1} for the isomer shifts, ±0.01 mm s^{-1} for the quadrupole splittings, ± 0.2 T for the hyperfine fields, and ± 1% for the relative areas. The absolute accuracies are approximately two to three times larger.

Results and Discussion

Chemical composition

The chemical analyses of $Na_2Mn_2Fe(PO_4)_3$ #1 and $Na_2MnFe^{II}Fe^{III}(PO_4)_3$ #4 are in fairly good agreement with the theoretical compositions, whereas the analysis of synthetic $NaMnFe_2(PO_4)_3$ #2, shows the presence of significant amounts of Fe^{II} (Table 1). In order to maintain charge balance, an excess of Mn was inserted in the structure, according to the substitution mechanism $\square$ + Na + $2Fe^{III}$ Na + Mn^{II} + $2Fe^{II}$ (Hatert

2002). The wet chemical analysis of natural NaMn $Fe_2(PO_4)_3$ #3 shows the presence of Al^{III}, Mg^{II}, and Ca^{II}, as has already been observed in several natural alluaudites. According to Moore and Ito (1979), Al^{III} and Mg^{II} are probably localized on the $M(2)$ site, whereas Ca^{II} is found in the channels of the structure.

By considering the cationic distribution among the different crystallographic sites according to the ionic radii of the cations (Shannon 1976), the structural formulas, $[A(2)'][A(1)]\ (M(1))\{M(2)_2\}(PO_4)_3$, of the four compounds investigated herein can be written as:

$[\square_{0.17}Na_{0.83}][Na_{1.00}](Na_{0.11}Mn_{0.89})\{Mn_{1.00}Fe^{III}_{1.00}\}(PO_4)_3$ #1,

$[\square_{0.91}Na_{0.09}][Na_{0.80}Mn_{0.20}](Mn_{1.00})\{Mn_{0.05}Fe^{II}_{0.22}Fe^{III}_{1.73}\}(PO_4)_3$ #2,

$[\square_{0.98}Na_{0.02}][Na_{0.73}Ca_{0.12}Mn_{0.15}](Mn_{1.00})\{Mn_{0.03}Fe^{II}_{0.11}Mg_{0.06}Fe^{III}_{1.67}Al_{0.13}\}(PO_4)_3$ #3, and

$[\square_{0.06}Na_{0.94}][Na_{0.91}Mn_{0.09}](Mn_{0.96}Fe^{II}_{0.04})\{Fe^{II}_{1.03}Fe^{III}_{0.97}\}(PO_4)_3$ #4.

These formulations have been used to calculate the magnetic properties of each of the four compounds, but otherwise the nominal $Na_2Mn_2Fe(PO_4)_3$ #1, NaMn $Fe_2(PO_4)_3$ #2 and #3, and $Na_2MnFe^{II}Fe^{III}(PO_4)_3$ #4, formulas will be used throughout this paper.

Structural properties

The X-ray single-crystal structure of the natural alluaudite from Buranga, #3, was determined by Moore (1971), and the X-ray single-crystal structure of synthetic $NaMnFe_2(PO_4)_3$ #2 was determined by Hatert et al. (2000). A Rietveld refinement of X-ray powder diffraction pattern of $Na_2Mn_2Fe^{II}\ Fe^{III}\ (PO_4)_3$ #4 was reported by Hatert et al. (2004).

The X-ray powder diffraction pattern of $Na_2Mn_2Fe(PO_4)_3$ #1 indicates that it is a pure alluaudite. The unit-cell parameters obtained from a Rietveld refinement, $a = 12.0372(7)$ Å, $b = 12.6231(7)$ Å, $c = 6.5103(4)$ Å, and $\beta = 114.545(1)°$, are in good agreement with those calculated with the LCLSQ 8.4 program (Table 2). The positional parameters and site occupancies, and interatomic distances and angles, obtained from the Rietveld refinements, are given in Tables 3 and 4, respectively. Both the satisfactory values of $R_p = 2.58$, $R_{wp} = 3.61$, $R_{Bragg} = 9.88$, and $S = 2.59$, and the mean O–P(1)–O and O–P(2)–O angles (Table 4), which are close to those of an ideal tetrahedron, confirm the reliability of the refinement. A polyhedral representation of the crystal structure of $Na_2Mn_2Fe(PO_4)_3$ #1, projected along the approximate [001] direction, is shown in Fig. 3.

The crystallographic sites (Table 3) of the alluaudite-like compounds are labeled according to the nomenclature recently proposed by Hatert et al. (2000). The morphologies of the coordination polyhedra of $M(1)$ and $M(2)$ are those of distorted octahedra, whereas the morphologies of $A(1)$ and $A(2)'$ are those of a distorted cube and of a gabled disphenoid, respectively. These morphologies are similar to those previously described for the $(Na_{1-x}Li_x)MnFe_2(PO_4)_3$ compounds (Hatert et al. 2000).

Because Fe and Mn cannot be distinguished by Rietveld refinements of X-ray data, the iron content of the $M(2)$ site is fixed to its theoretical value (Table 3). A preliminary refinement, performed assuming Mn^{II} on $M(1)$ and Na^{I} on $A(1)$ and $A(2)'$, indicates a rather low electronic density on $M(1)$ and a rather high electronic density on $A(1)$, as compared with the theoretical values. This behavior is most likely related to the presence of small amounts of Na^{I} on the $M(1)$ site and of Mn^{II} on the $A(1)$ site. Consequently, the occupancy factors for the $A(1)$ and $M(1)$ sites (Table 3) are calculated assuming a full occupancy by Na^{I} and Mn^{II}. Several refinements were performed in order to evaluate the influence of the thermal factor, B, on the site occupancy factors. When B is fixed to the values of 0.5 and 1.0, the occupancy factors of $M(1)$ are 0.447 Mn^{II} + 0.054 Na^{I} and 0.459 Mn^{II} + 0.042 Na^{I}, and those of $A(1)$ are 0.493 Na^{I} + 0.008 Mn^{II} and 0.485 Na^{I} + 0.015 Mn^{II}, respectively. Consequently, within the range of acceptable B values, the occupancy factors confirm a disordered distribution of Na^{I} and Mn^{II} on the $M(1)$ and $A(1)$ crystallographic sites. A similar disordered distribution has already been observed by Hatert (2002) in the alluaudite-like compound, $Na_2Mn_2\ Ga(PO_4)_3$, and by Hatert et al. (2004) in the $Na_2(Mn_{1-x}Fe^{II}_x)_2Fe^{III}(PO_4)_3$ alluaudites, where x is 0.00 to 0.25.

Because of their importance in determining the magnetic exchange interactions, see below, the $M(1)$–O(1)–$M(2)$, $M(1)$–O(3)–$M(2)$, and $M(2)$–O(5)–$M(2)$ bond angles involving the magnetic cations have been determined and are given in Table 5. It is immediately apparent in this table that the weighted average of these bond angles is smaller by ~2° in $Na_2Mn_2Fe(PO_4)_3$ #1 than in the remaining three compounds. Further, because of the importance of the cation site distortion in determining the Mössbauer spectral quadrupole splittings (see below) the bond length and angle distortion

Table 2 The unit-cell parameters for synthetic and natural alluaudites

Parameter	$Na_2Mn_2Fe(PO_4)_3$ #1, synthetic	$NaMnFe_2(PO_4)_3$ #2, synthetic	$NaMnFe_2(PO_4)_3$ #3, natural	$Na_2MnFe_2(PO_4)_3$ #4, synthetic
a, Å	12.048(3)	12.010(3)	12.006(2)	11.944(2)
b, Å	12.623(2)	12.530(3)	12.525(2)	12.560(2)
c, Å	6.511(1)	6.407(2)	6.394(1)	6.480(1)
β, deg	114.58(2)	114.54(2)	114.30(1)	114.52(1)
V, Å^3	900.5(2)	877.2(3)	876.3(2)	884.4(2)

Table 3 Positional, isotropic thermal, and site occupancy parameters for the synthetic alluaudite-type compound $Na_2Mn_2Fe(PO_4)_3$ #1

Site	Atom	Wyckoff	*x*	*y*	*z*	*B* (Å^2)	*N*
A(2)′	Na	4*e*	0	−0.0145(8)	1/4	1.0	0.411(3)
A(1)	Na	4*b*	1/2	0	0	1.0	0.485(4)
	Mn	4*b*	1/2	0	0	1.0	0.015(4)
M(1)	Mn	4*e*	0	0.2742(4)	1/4	0.5	0.448(7)
	Na	4*e*	0	0.2742(4)	1/4	0.5	0.052(7)
M(2)	Mn	8*f*	0.2825(3)	0.6580(2)	0.3590(6)	0.5	0.500(6)
	Fe	8*f*	0.2825(3)	0.6580(2)	0.3590(6)	0.5	0.5
P(1)	P	4*e*	0	−0.2885(5)	1/4	0.5	0.5
P(2)	P	8*f*	0.2325(5)	−0.1110(4)	0.130(1)	0.5	1.0
O(1)	O	8*f*	0.4659(7)	0.7244(6)	0.557(2)	1.0	1.0
O(2)	O	8*f*	0.0939(9)	0.6360(6)	0.215(1)	1.0	1.0
O(3)	O	8*f*	0.3256(7)	0.6614(6)	0.108(1)	1.0	1.0
O(4)	O	8*f*	0.1366(7)	0.4080(6)	0.329(1)	1.0	1.0
O(5)	O	8*f*	0.2289(7)	0.8335(6)	0.342(2)	1.0	1.0
O(6)	O	8*f*	0.3238(6)	0.4983(8)	0.391(1)	1.0	1.0

Table 4 Selected interatomic distances (Å) and angles (°) for the synthetic alluaudite-type compound, $Na_2Mn_2Fe(PO_4)_3$ #1

A(2)′–O(6) × 2	2.426(6)	*M*(2)–O(1)–*M*(1)	95.4(5)
A(2)′–O(6) × 2	2.645(5)	*M*(2)–O(3)–*M*(1)	101.0(3)
A(2)′–O(1) × 2	2.89(1)	*M*(2)–O(5)–*M*(2) × 2	97.8(4)
A(2)′–O(3) × 2	2.93(1)	Mean	98.1
Mean	2.72		
		P(1)–O(1) × 2	1.41(1)
A(1)–O(2) × 2	2.207(7)	P(1)–O(2) × 2	1.567(9)
A(1)–O(4) × 2	2.390(6)	Mean	1.49
A(1)–O(4) × 2	2.612(6)		
A(1)–O(2) × 2	3.069(7)	O(2)–P(1)–O(2)	105.1(5)
Mean	2.57	O(1)–P(1)–O(2) × 2	100.4(3)
		O(1)–P(1)–O(1)	109.7(7)
M(1)–O(4) × 2	2.263(8)	O(1)–P(1)–O(2) × 2	121.4(3)
M(1)–O(1) × 2	2.29(1)	Mean	109.7
M(1)–O(3) × 2	2.383(7)		
Mean	2.31	P(2)–O(6)	1.52(1)
		P(2)–O(4)	1.505(7)
M(2)–O(6)	2.07(1)	P(2)–O(3)	1.547(9)
M(2)–O(2)	2.085(8)	P(2)–O(5)	1.57(1)
M(2)–O(3)	1.910(7)	Mean	1.54
M(2)–O(5)	2.01(1)		
M(2)–O(1)	2.208(8)	O(3)–P(2)–O(4)	104.3(4)
M(2)–O(5)	2.297(8)	O(4)–P(2)–O(6)	105.5(5)
Mean	2.10	O(3)–P(2)–O(6)	106.5(5)
		O(4)–P(2)–O(5)	109.1(5)
M(1)–*M*(2)	3.327(3)	O(5)–P(2)–O(6)	108.1(4)
		O(3)–P(2)–O(5)	122.2(5)
		Mean	109.3

parameters (Renner and Lehmann 1986) for the *M*(1) and *M*(2) sites were calculated and are given in Table 6. Again, it is immediately apparent in Table 6 that, for both the *M*(1) and *M*(2) sites, the bond length distortion is larger and the bond-angle distortion is smaller in $Na_2Mn_2Fe(PO_4)_3$ #1 than in the remaining three compounds. The incorporation of a large amount of Mn^{+2} in the *M*(2) site of the alluaudite structure is probably responsible for the significant distortion of this site and for the change in the M–O–M angles. The significant distortion of the P(1) site (Table 4) probably results from the location of this site within the (010) plane which contains the octahedral chains of the structure. A refinement with a constraint applied to the P(1)–O(1) distance was also tried, but the *R* values increase significantly, and become unacceptable.

Magnetic properties

The magnetic properties of synthetic $Na_2Mn_2Fe(PO_4)_3$ #1, synthetic $NaMnFe_2(PO_4)_3$ #2, natural $NaMnFe_2(PO_4)_3$ #3, and synthetic $Na_2MnFe^{II}Fe^{III}(PO_4)_3$ #4 were measured between 4.2 and 295 K and the magnetic properties of the four compounds, calculated from their analytical formulations, are summarized in Table 7. The molar magnetic susceptibility of all four compounds increases uniformly upon cooling such that the inverse magnetic susceptibility (Fig. 4), is linear above ~40 K. In this figure the linear extrapolation to zero yields the Weiss temperature, θ, given in Table 7. Below 40 K the inverse susceptibility decreases below that expected of a paramagnetic compound, a decrease which is indicative of a weak ferromagnetic component to the susceptibility. This ferromagnetic component arises from a canting of the antiferromagnetically coupled moments by the 4 T applied field. The magnetization has also been measured as a function of applied field up to fields of 4 T. In all four compounds and at all temperatures studied the magnetization increased linearly with applied field and, even at 4.2 K, no hysteresis in the magnetization was observed.

Plots of χ_MT vs. T (not shown) indicate that, in all four compounds, χ_MT decreases monotonically upon cooling; there is no indication of any shoulder or peak at lower temperatures in #2–4 although #1 does show a broad shoulder below 30 K. Thus, except for the missing shoulder in #2–4, the magnetic properties of all the compounds are very similar to those observed by Chouaibi et al. (2001) for the alluaudite-like $Ag_2FeMn_2(PO_4)_3$ compound. They attribute the presence of a peak at 19 K in the χ_MT vs. T plot for $Ag_2FeMn_2(PO_4)_3$ to weak ferromagnetism below 19 K, ferromagnetism which results from a canting of the antiferromagnetically coupled spins.

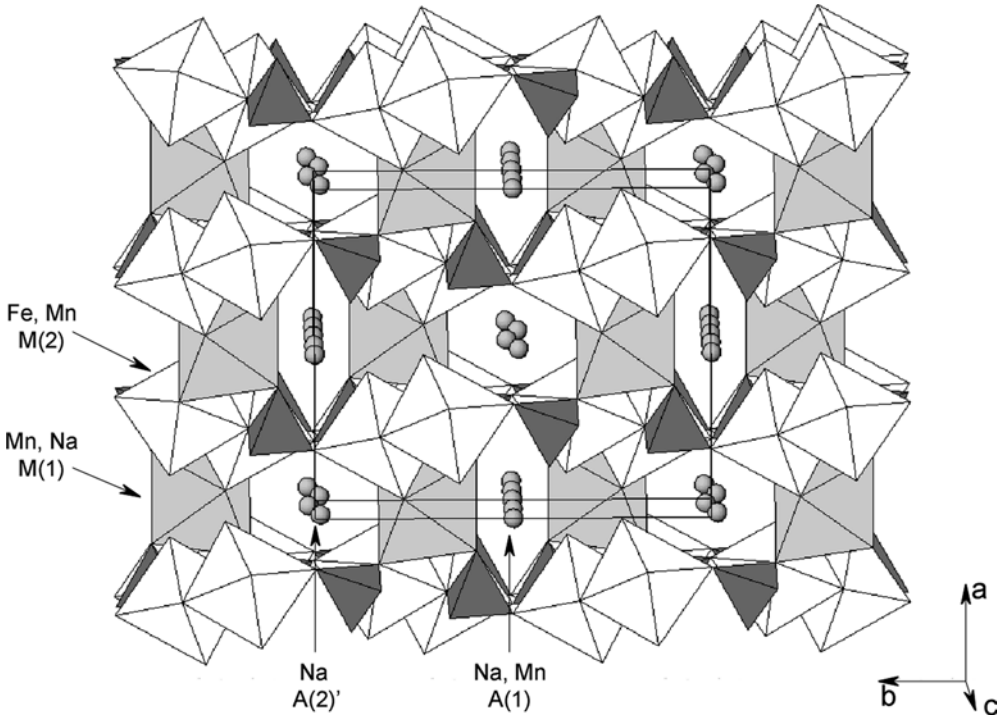

Fig. 3 A projection of the crystal structure of $Na_2Mn_2Fe(PO_4)_3$ #1. The PO_4 tetrahedra are *darkly shaded*. The *shaded* $M(1)$ octahedra are occupied by Mn and Na, and the *unshaded* $M(2)$ octahedra are occupied by Fe^{III} and Mn. The *circles* indicate Na and Mn at the $A(1)$ site, and Na at the $A(2)$' crystallographic site

The effective magnetic moment, μ_{eff}, per formula unit for compouds #1–4 has been calculated as a function of temperature (Fig. 5). The observed moments indicate that all the compounds are paramagnetic above ~40 K and, further the moments of #2 and #3 are, to a first approximation, those expected of high-spin $S = 5/2$ manganese (II) and iron (III). Typically, for these ions, one would expect to observe a temperature-independent spin-only effective magnetic moment, μ_{eff}, of 5.92 μ_B. Indeed, this is close to what is observed for both natural and synthetic $NaMnFe_2(PO_4)_3$ #2 and #3, whose moments per cation are 6.02 and 6.00 μ_B between 50 and 295 K. Thus, it seems that these compounds are paramagnetic with essentially no exchange coupling between the magnetic cations above 50 K. The difference between the effective magnetic moment and that calculated by assuming temperature independent moments of 5.92 μ_B for manganese(II) and iron(III) and 5.20 μ_B for iron(II) is shown in the inset of Fig. 5.

Below 50 K the effective magnetic moments of both #2 and #3 begin to increase slightly, (Fig. 5), and exhibit a small peak or shoulder at ca. 35 and 30 K, respectively, a peak which is reminiscent of weak antiferromagnetic coupling. Then, at lower temperatures the moments increase significantly to values of ~11.53 and 11.78 μ_B, respectively, at 4.2 K. This low-temperature behavior is typical of either weak ferromagnetic exchange coupling between the magnetic cations or a canting of antiferromagnetic moments in the applied field of 4 T. It should be noted that in #2 and #3, 19 and 10% of the iron(III) has been reduced to high-spin, $S = 2$, iron(II). Any high-spin iron(II) present will tend to reduce the average moment and the increasing amount of iron(II) probably accounts for why the moment of #2 is slightly lower than that of #3.

The presence of 50% of iron(II) and 50% of iron(III) also accounts for why the observed moment of $Na_2MnFe^{II}Fe^{III}(PO_4)_3$ #4 is smaller than that of #2 and #3. Indeed, if one assumes a high-spin iron(II) moment of 5.20 μ_B, a value which includes a small orbital contribution to the moment, the average value for the moment per formula unit expected for #4 is 9.99 μ_B, a value which agrees well with the moment of 10.08 μ_B observed between 50 and 300 K. Further, it is well known (Long and Baker 1971) that the moment of high-spin iron(II) in a distorted octahedral environment will show a small temperature dependence, often with a

Table 5 Selected *M–O–M* bond angles, in degrees, for synthetic and natural alluaudites

	$Na_2Mn_2Fe(PO_4)_3$ #1, synthetic	$NaMnFe_2(PO_4)_3$ #2, synthetic	$NaMnFe_2(PO_4)_3$ #3, natural	$Na_2MnFe_2(PO_4)_3$ #4, synthetic
$M(1)$–O(1)–$M(2)$	95.4(5)	103.44(5)	103.1(3)	100.8(3)
$M(1)$–O(3)–$M(2)$	101.0(3)	102.44(5)	101.9(3)	104.7(3)
$M(2)$–O(5)–$M(2)$	97.8(4) × 2	97.40(5) × 2	97.4(3) × 2	96.6(3) × 2
Weighted average	98.07	100.17	99.95	99.68

Table 6 Bond length and angle distortion parameters for the $M(1)$ and $M(2)$ sites of the synthetic and natural alluaudites

Parameter	$Na_2Mn_2Fe(PO_4)_3$ #1, synthetic	$NaMnFe_2(PO_4)_3$ #2, synthetic	$NaMnFe_2(PO_4)_3$ #3, natural	$Na_2MnFe_2(PO_4)_3$ #4, synthetic
Length distortion[a]				
$M(1)$	2.05	1.27	1.22	1.53
$M(2)$	4.97	3.14	3.03	2.79
Angle distortion[b]				
$M(1)$	11.06	12.91	13.07	12.73
$M(2)$	7.35	9.02	8.77	8.26

$$\text{Length distortion} = \frac{100}{M} \cdot \sum_{i=1}^{m} \frac{|d_i - d_m|}{d_m} \quad (1)$$

$$\text{Angle distortion} = \frac{100}{M} \cdot \sum_{i=1}^{m} \frac{|a_i - a_m|}{a_m} \quad (2)$$

where n is the number of bonds, d_m and a_m are the mean bond length and angle, respectively, and d_i and a_i are the individual bond lengths and angles, respectively

Table 7 The magnetic properties of synthetic and natural alluaudites

Parameter	$Na_2Mn_2Fe(PO_4)_3$ #1, synthetic	$NaMnFe_2(PO_4)_3$ #2, synthetic	$NaMnFe_2(PO_4)_3$ #3, natural	$Na_2MnFe_2(PO_4)_3$ #4, synthetic
Mol wt, g mol^{-1}	489.19	482.95	476.17	499.06
$\chi_{M,\ \text{dia. corr.}}$, emu mol^{-1}	0.000193	0.000189	0.000187	0.000195
C, K/(emu mol^{-1})[a]	11.37 ± 0.01	13.600 ± 0.004	13.50 ± 0.01	12.71 ± 0.01
θ, K[b]	−40.6 ± 0.2	−64.80 ± 0.05	−61.3 ± 0.2	−37.2 ± 0.1
T_N, K	40 ± 5	35 ± 2	32 ± 2	32 ± 2
μ_{eff}, μ_B[c]	9.537 ± 0.005	10.429 ± 0.002	10.392 ± 0.004	10.084 ± 0.006
μ_{eff}, μ_B[d]	5.51	6.02	6.00	5.82
μ_{eff}, μ_B at 4.2 K	12.20	11.53	11.78	9.85

[a] The Curie constant obtained from a fit of the molar magnetic susceptibility for the data measured between 50 and 300 K
[b] The Weiss temperature obtained from a fit of the inverse molar magnetic susceptibility for the data measured between 50 and 300 K. The *error bars* represent the statistical error; the experimental error may be larger by a factor of 5 to 10
[c] The effective magnetic moment per formula unit obtained from the Curie constant. The *error bars* represent the statistical error; the experimental error may be larger by a factor of 5 to 10
[d] The average effective magnetic moment per magnetic cation obtained from the Curie constant

maximum in the moment below room temperature. Thus, the presence of iron(II) in its low-symmetry coordination environment may well account for the weak maximum in the moment observed at ~120 K. Again, #4 shows a weak peak in its moment at ~35 K, decreases to a minimum of 9.5 μ_B at 20 K, and finally upon further cooling to 4.2 K, increases slightly to 9.8 μ_B as a result of spin canting in the 4 T applied field.

The magnetic properties of $Na_2Mn_2Fe(PO_4)_3$ #1 are rather different from those of #2, #3, and #4. This compound which contains three $S = 5/2$ ions, i.e., two high-spin manganese(II) and one high-spin iron(III) ions, ions which would be expected to yield a temperature-independent moment of 5.92 μ_B per cation or 10.25 μ_B per formula unit. In contrast, the Curie constant yields a moment of 9.51 μ_B between 50 and 295 K and a broad maximum of 9.55 μ_B is observed at ~200 K and then decreases to ~9.47 μ_B before increasing below ~40 K. This behavior is typical of a compound undergoing short-range antiferromagnetic coupling above 40 K and ferromagnetic canting of the antiferromagnetically ordered moments below 40 K. Indeed, of compounds #1–4, $Na_2Mn_2Fe(PO_4)_3$ #1 has M–O–M bond angles, especially the $M(1)$–O(1)–$M(2)$ bond angle (Table 5) which are closest to 90°, the angle at which antiferromagnetic exchange coupling is most favorable (Goodenough 1963). Further, as would be expected, #1 shows the largest deviations from the Curie–Weiss plot between 50 and 300 K.

Mössbauer spectral properties

Paramagnetic spectra

The Mössbauer spectra of synthetic $Na_2Mn_2Fe(PO_4)_3$ #1, synthetic $NaMnFe_2(PO_4)_3$ #2, natural $NaMnFe_2(PO_4)_3$ #3, and synthetic $Na_2MnFe^{II}Fe^{III}(PO_4)_3$ #4 have been measured between 4.2 and 295 K and the spectra obtained at 80 K are shown in Fig. 6. Selected

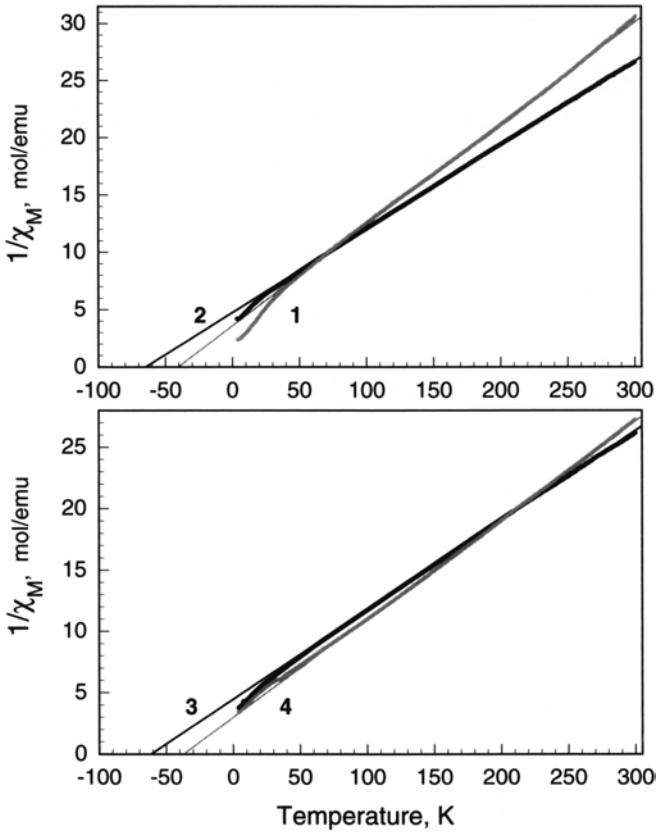

Fig. 4 The inverse magnetic susceptibility as a function of temperature obtained at 4 T for $Na_2Mn_2Fe(PO_4)_3$ *#1*, synthetic NaMn $Fe_2(PO_4)_3$ *#2*, natural $NaMnFe_2(PO_4)_3$ *#3*, and $Na_2MnFe^{II}Fe^{III}(PO_4)_3$ *#4*. The linear fits are to the data obtained between 50 and 300 K

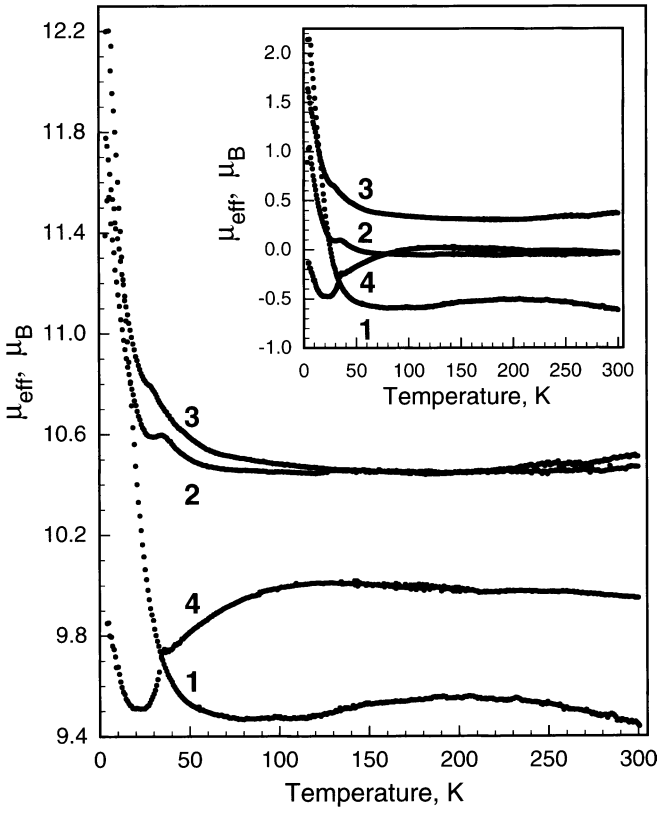

Fig. 5 The effective magnetic moment, μ_{eff}, per formula unit of $Na_2Mn_2Fe(PO_4)_3$ *#1*, synthetic $NaMnFe_2(PO_4)_3$ *#2*, natural NaMn $Fe_2(PO_4)_3$ *#3*, and $Na_2MnFe^{II}Fe^{III}(PO_4)_3$ *#4*, obtained at an applied field of 4 T. *Inset* The difference between the effective magnetic moment and that calculated by assuming temperature-independent moments of 5.92 μ_B for manganese(II) and iron(III) and 5.20 μ_B for iron(II)

Mössbauer spectral hyperfine parameters for the four compounds are given in Table 8. The fits shown in this Fig. 6 are based upon a binomial distribution of near-neighbor environments of iron on the $M(2)$ sites resulting from a random distribution of Mn^{II}, Fe^{II}, and Fe^{III} on the adjacent $M(2)$ sites, a binomial distribution which has been used earlier (Hatert et al. 2003, 2004; Hermann et al. 2002) to fit related spectra. In all cases it has been assumed that the $M(1)$ site is 100% occupied by Mn^{II}, an assumption that is perfect for samples #2 and #3, and very good for #1 and #4, according to the chemical analyses. The presence of Fe^{II} on the $M(1)$ site cannot definitely be ruled out for sample #2, but it seems more meaningful to include Mn^{II} on this site because of its larger ionic radius. For samples #1 and #4, the percentage spectral areas observed for the iron(II) doublets are in good agreement with the chemical analyses, see Table 9. However, for samples #2 and #3, the percentage spectral areas observed for the iron(II) doublets are significantly larger than the percentages obtained from the chemical analyses, probably as a result of partial oxidation during these analyses.

Because of the large observed isomer shift and quadrupole splitting of iron(II), it is possible to determine the relative amount of iron(II) in all four of the compounds from the area of the iron(II) doublet component found at ~2.7 mm s^{-1}, (Fig. 6). As expected, no iron(II) component is observed in #1, an unexpected but small amount of iron(II) is found in #2 and #3, and, as expected, approximately one-half of the iron in #4 is iron(II). In all the additional spectral fits of the paramagnetic spectra obtained at other temperatures the amount of iron(II) has been constrained to that observed at 80 K (see Fig. 6), a constraint that works perfectly for #2 and #3 at all temperatures and for #4 below 200 K. In the latter case, above 200 K, as a consequence of the expected lower recoil-free fraction for the iron(II) as compared to iron(III), the constraint on the iron(II) relative area slightly overestimates the amount of iron(II).

In agreement with our earlier work (Hatert et al. 2003, 2004; Hermann et al. 2002), the iron(II) doublet with the largest quadrupole splitting (Fig. 6) is assigned to iron(II) on the $M(2)$ site which has an iron(III) neighbor on its adjacent $M(2)$ site, whereas the weaker iron(II) doublet with a somewhat smaller quadrupole splitting is assigned to iron(II) with an iron(II) neighbor on its adjacent $M(2)$ site. Further, the most intense

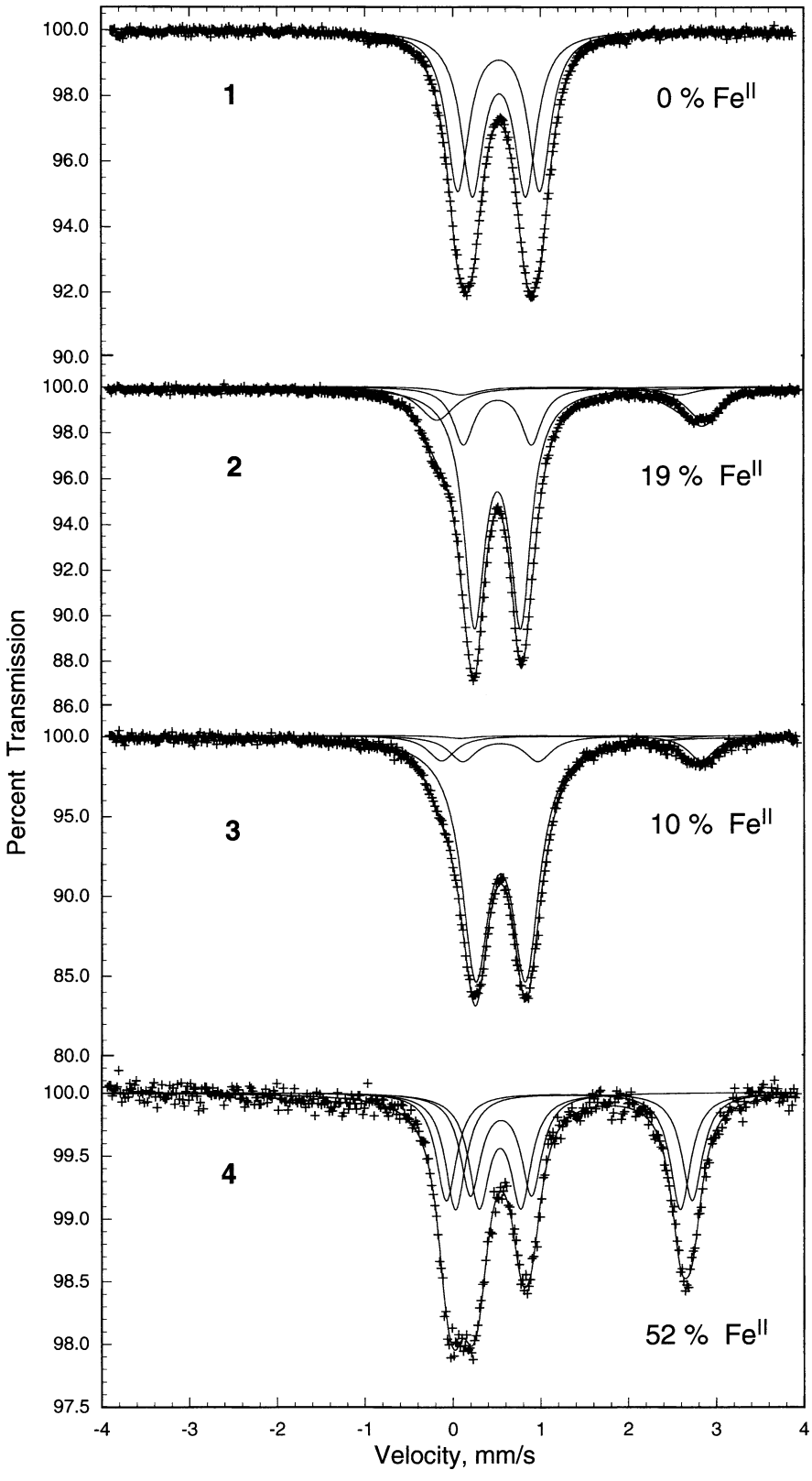

Fig. 6 The Mössbauer spectra of $Na_2Mn_2Fe(PO_4)_3$ #1, synthetic $NaMnFe_2(PO_4)_3$ #2, natural $NaMnFe_2(PO_4)_3$ #3, and $Na_2MnFe^{II}Fe^{III}(PO_4)_3$ #4, obtained at 80 K. The relative spectral absorption area of the iron(II) observed in each spectrum is indicated

iron(III) doublet is assigned to iron(III) on the $M(2)$ site, which has an iron(III) neighbor on its adjacent $M(2)$ site, whereas the substantially weaker iron(III) doublet is assigned to iron(III) with an iron(II) neighbor on its adjacent $M(2)$ site. The values of the corresponding isomer shifts and quadrupole splittings, see Table 8, are consistent with both the expected local $M(2)$ site structural and elemental environment and with our earlier

Table 8 Selected Mössbauer spectral parameters for the paramagnetic natural and synthetic alluaudites

Compound	*T*, K	δ, mm/s[a]	ΔE_Q, mm/s^{-1}	$<\Delta E_Q>$, mm/s^{-1}	Ggr;, mm/s^{-1}	*Area*, %	Assign-ment	*M*(2) near-neighbor
$Na_2Mn_2Fe(PO_4)_3$ #1, Synthetic	295	0.424	0.92	0.76	0.29	50	Fe^{III}	Mn^{II}
		0.424	0.60	–	0.29	50	Fe^{III}	Fe^{III}
	80	0.528	0.93	0.92	0.31	50	Fe^{III}	Mn^{II}
		0.528	0.61	–	0.31	50	Fe^{III}	Fe^{III}
$NaMnFe_2(PO_4)_3$ #2, Synthetic	295	1.250	1.99	2.52	0.57	3.8	Fe^{II}	Fe^{II}
		1.250	2.65	–	0.57	15.2	Fe^{II}	Fe^{III}
		0.430	0.78	0.57	0.35	16.2	Fe^{III}	Fe^{II}
		0.430	0.52	–	0.35	64.8	Fe^{III}	Fe^{III}
	80	1.332	2.73	3.01	0.37	3.8	Fe^{II}	Fe^{II}
		1.332	3.08	–	0.37	15.2	Fe^{II}	Fe^{III}
		0.533	0.82	0.58	0.31	16.2	Fe^{III}	Fe^{II}
		0.533	0.52	–	0.31	64.8	Fe^{III}	Fe^{III}
	45	1.361	2.74	3.03	0.37	3.8	Fe^{II}	Fe^{II}
		1.361	3.10	–	0.37	15.2	Fe^{II}	Fe^{III}
		0.542	0.81	0.59	0.31	16.2	Fe^{III}	Fe^{II}
		0.542	0.53	–	0.31	64.8	Fe^{III}	Fe^{III}
$NaMnFe_2(PO_4)_3$ #3, Natural	295	1.217	2.21	2.44	0.53	1.0	Fe^{II}	Fe^{II}
		1.217	2.47	–	0.53	9.0	Fe^{II}	Fe^{III}
		0.433	0.85	0.58	0.35	9.0	Fe^{III}	Fe^{II}
		0.433	0.55	–	0.35	81.0	Fe^{III}	Fe^{III}
	80	1.350	2.53	2.92	0.38	1.0	Fe^{II}	Fe^{II}
		1.350	2.96	–	0.38	9.0	Fe^{II}	Fe^{III}
		0.540	0.86	0.60	0.38	9.0	Fe^{III}	Fe^{II}
		0.540	0.57	–	0.38	81.0	Fe^{III}	Fe^{III}
	45	1.367	2.51	3.02	0.37	1.0	Fe^{II}	Fe^{II}
		1.367	3.08	–	0.37	9.0	Fe^{II}	Fe^{III}
		0.539	0.84	0.61	0.37	9.0	Fe^{III}	Fe^{II}
		0.539	0.58	–	0.37	81.0	Fe^{III}	Fe^{III}
$Na_2MnFe_2(PO_4)$ #4, Synthetic	295	1.172	2.13	2.23	0.44	27.03	Fe^{II}	Fe^{II}
		1.172	2.34	–	0.44	24.96	Fe^{II}	Fe^{III}
		0.459	0.57	0.46	0.34	24.96	Fe^{III}	Fe^{II}
		0.459	0.34	–	0.34	23.04	Fe^{III}	Fe^{III}
	80	1.316	2.58	2.69	0.29	27.03	Fe^{II}	Fe^{II}
		1.316	2.80	–	0.29	24.96	Fe^{II}	Fe^{III}
		0.539	0.69	0.58	0.28	24.96	Fe^{III}	Fe^{II}
		0.539	0.47	–	0.28	23.04	Fe^{III}	Fe^{III}
	35	1.325	2.57	2.69	0.26	27.03	Fe^{II}	Fe^{II}
		1.325	2.83	–	0.26	24.96	Fe^{II}	Fe^{III}
		0.546	0.71	0.59	0.28	24.96	Fe^{III}	Fe^{II}
		0.546	0.47	–	0.28	23.04	Fe^{III}	Fe^{III}

[a] The isomer shifts are given relative to room temperature α-iron foil.

Table 9 The iron composition of the synthetic and natural alluaudites

Parameter	Method	$Na_2Mn_2Fe(PO_4)_3$ #1, synthetic	$NaMnFe_2(PO_4)_3$ #2, synthetic	$NaMnFe_2(PO_4)_3$ #3, natural	$Na_2MnFe_2(PO_4)_3$ #4, synthetic
Fe^{II}, % of total Fe	Chemical analysis	0	12	6	52
Fe^{II}, % area	Mössbauerspectroscopy	0	18(2)	10	52
Fe^{II}/Fe^{III}	Chemical analysis	0	0.12	0.06	1.08
Fe^{II}/Fe^{III}	Mössbauerspectroscopy	0	0.22	0.11	1.08

work. Preliminary fits indicated that the isomer shifts and line widths for two iron(II) and two iron(III) sites were essentially identical and subsequently they have been constrained to be equal.

In order to further confirm the spectral assignments shown in Fig. 6, the various spectra obtained between 295 K and the ordering temperature (see below) have been successfully fitted with the same binomial model. The paramagnetic spectra of synthetic $Na_2Mn_2Fe(PO_4)_3$ #1 are virtually the same as that shown in Fig. 6, except for the expected variation in the spectral absorption area. The temperature dependence of the paramagnetic Mössbauer spectra of synthetic $NaMnFe_2(PO_4)_3$ #2 is shown in Fig. 7. The paramagnetic spectra of natural

$NaMnFe_2(PO_4)_3$ #3 are virtually identical to those shown in Fig. 7 except for a small reduction in the amount of iron(II) present. The temperature dependence of the paramagnetic Mössbauer spectra of synthetic $Na_2MnFe^{II}Fe^{III}(PO_4)_3$ #4 is shown in Fig. 8.

The essentially linear temperature dependencies of the isomer shifts in $NaMnFe_2(PO_4)_3$ #2 and $Na_2MnFe^{II}Fe^{III}(PO_4)_3$ #4 are shown in Fig. 9. The results obtained for natural $NaMnFe_2(PO_4)_3$ #3 are virtually identical to those obtained for synthetic $NaMnFe_2(PO_4)_3$ #2 (Fig. 9). The isomer shifts for the iron(III) site are quite similar in all four compounds, but, in contrast (Fig. 9), the iron(II) isomer shift in #2 (as well as in #3) is significantly higher than in #4, a difference that cannot be attributed to differences in the $M(2)$ iron(II) to oxygen bond distances. On the basis of these bond distances, one would expect the reverse order for the iron(II) isomer shifts. Thus, the observed differences in the iron(II) isomer shifts must be due to the presence of substantially more iron(II) on the $M(2)$ sites in #4 as compared to #2 and #3. Indeed, the added electron associated with the iron(II) $M(2)$ near neighbor may well increase, at least in part, the *s*-electron density at the adjacent edge-sharing $M(2)$ iron(II) site, an increase that will reduce the isomer shift.

The temperature dependence of the quadrupole splittings in $NaMnFe_2(PO_4)_3$ #2, and $Na_2MnFe^{II}Fe^{III}(PO_4)_3$ #4, is shown in Fig. 10. The temperature dependence of the quadrupole splittings observed for natural $NaMnFe_2(PO_4)_3$ #3 is essentially the same as that of #2 shown in Fig. 10. It should be noted that the larger quadrupole splitting observed for $NaMnFe_2(PO_4)_3$ #2, as compared to that of $Na_2MnFe^{II}Fe^{III}(PO_4)_3$ #4, is a consequence of the larger distortion from that of perfect octahedral coordination of both the bond length and bond angle distortion (Table 6), in the former compound. Further, a site which has iron of the same oxidation state on its neighboring $M(2)$ site has a smaller quadrupole splitting than when the oxidation states are different, an indication of an added distortion to the coordination environment in the latter case.

The temperature dependence of the iron(II) quadrupole splittings for #2 and #4 (Fig. 10), has been fitted with the Ingalls' model (1964) with the Eq. (1),

$$\Delta E_Q = \Delta E_Q(0) \times \{1 - \exp(-\Delta E/\mathrm{k}T)\}/ \{1 + 2\exp(-\Delta E/\mathrm{k}T)\}, \quad (1)$$

where $\Delta E_Q(0)$ is the quadrupole splitting at zero Kelvin and ΔE is the low-symmetry component in the pseudo-octahedral iron(II) crystal-field splitting. The low-symmetry crystal-field splitting, ΔE, is 560 ± 5 cm^{-1} for the two iron(II) sites in $Na_2MnFe^{II}Fe^{III}(PO_4)_3$ #4, whereas in $NaMnFe_2(PO_4)_3$ #2, the splitting is 606 ± 10 cm^{-1} for the iron(II) site when it has an iron(III) near neighbor and 443 ± 10 cm^{-1} when it has an iron(II) near neighbor on the $M(2)$ site. As might be expected for the presence of In^{III} on the $M(2)$ site or Li^{I} on the A sites, these values are smaller than the ~650 cm^{-1} values obtained for $NaMnFeIn(PO_4)_3$ by Hatert et al. (2003) and the ~685 cm^{-1} values obtained for $Na_{0.5}Li_{0.5}MnFe_2(PO_4)_3$ by Hermann et al. (2002). Similar values of ~500 to 600 cm^{-1} have been obtained by Hatert et al. (2004) for $Na_2(Mn_{1-x}Fe_x^{II})_2Fe^{III}(PO_4)_3$, in which iron(II) is found on both the $M(1)$ and $M(2)$ sites.

Thus, it appears that the presence of the unexpected, but small, amount of iron(II) in #2 yields a reduction in the electronic distortion at its near-neighbor iron(II). The poorer fit obtained with Eq. (1) for the temperature dependence of the quadrupole splitting in $NaMnFe_2(PO_4)_3$ #2, as compared to that of $Na_2MnFe^{II}Fe^{III}(PO_4)_3$ #4, may be an indication of either a structural change occurring in #2 upon cooling, or the presence of a trigonal component to the crystal field (Varret et al. 1972), cases that are not considered in the Ingalls' model. A fit with the Ingalls' model for a rhombic distortion of the crystal field was unsuccessful, presumably because of the paucity of data points.

Antiferromagnetically ordered Mössbauer spectra.

A close inspection of Figs. 7 and 8 reveals that the paramagnetic Mössbauer spectra of synthetic $NaMnFe_2(PO_4)_3$ #2 and $Na_2MnFe^{II}Fe^{III}(PO_4)_3$ #4 begin to broaden at 35 and 32 K, respectively, as a result of long-range antiferromagnetic ordering, an ordering which is consistent with the observed decrease in the inverse magnetic susceptibilities (Fig. 4). Natural $NaMnFe_2(PO_4)_3$ #3 also shows the onset of ordering at 32 K. This antiferromagnetic ordering is confirmed by the Mössbauer spectra of #2–4 obtained below the ordering temperatures, see Figs. 11–13, spectra which show the sextets characteristic of antiferromagnetically ordered compounds.

The antiferromagnetically ordered Mössbauer spectra have been fitted with the requisite number of magnetic sextets and quadrupole doublets needed to reproduce the observed spectra, and the resulting hyperfine parameters of the magnetic components are given in Table 10. In some spectra the paramagnetic and magnetically ordered spectra coexist over a small range of temperatures (see, for example, the 25 K spectra in Figs. 11–13), and the hyperfine parameters for the paramagnetic doublets have been constrained to those observed just above the ordering temperature. Further, it should be noted in Figs. 11 and 12 that, at 4.2 and 15 K, the respective 19 and 10% area of the presumably ordered iron(II) sextets is not observed; apparently these sextets are so broad perhaps because of relaxation that they are hidden in the background of the iron(III) spectra. Indeed, in $NaMnFe_2(PO_4)_3$ #3, the 2% effect observed for the iron(II) quadrupole doublet component would lead to a magnetic sextet component of approximately 1%, a component that one would expect to observe in Fig. 12. Thus, its absence is a good indication that the iron(II) sextets are relaxation-broadened even at 4.2 K. At 4.2 and 15 K it has proven possible to fit the

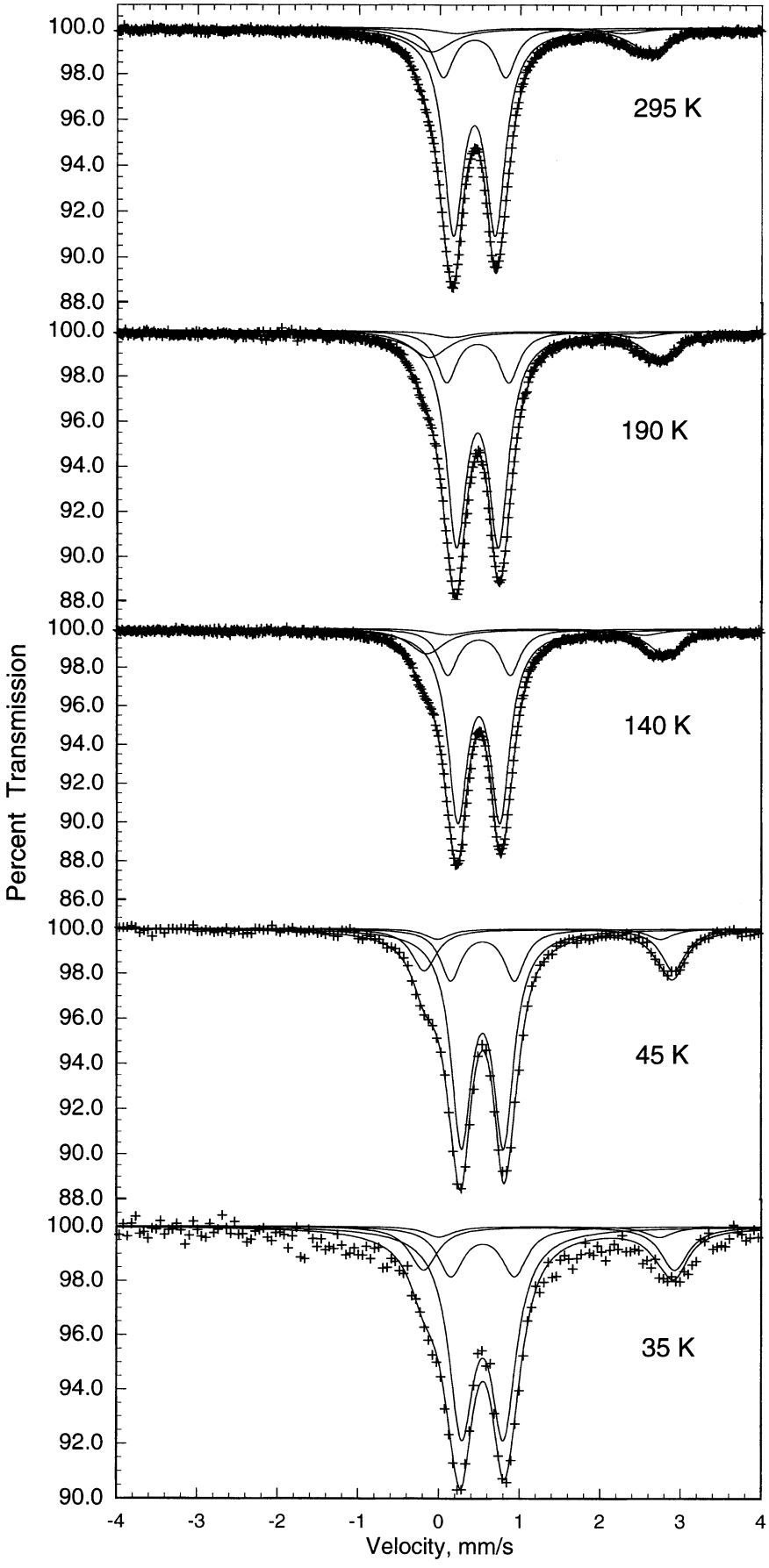

Fig. 7 The temperature dependence of the paramagnetic Mössbauer spectra of synthetic $NaMnFe_2(PO_4)_3$ #2

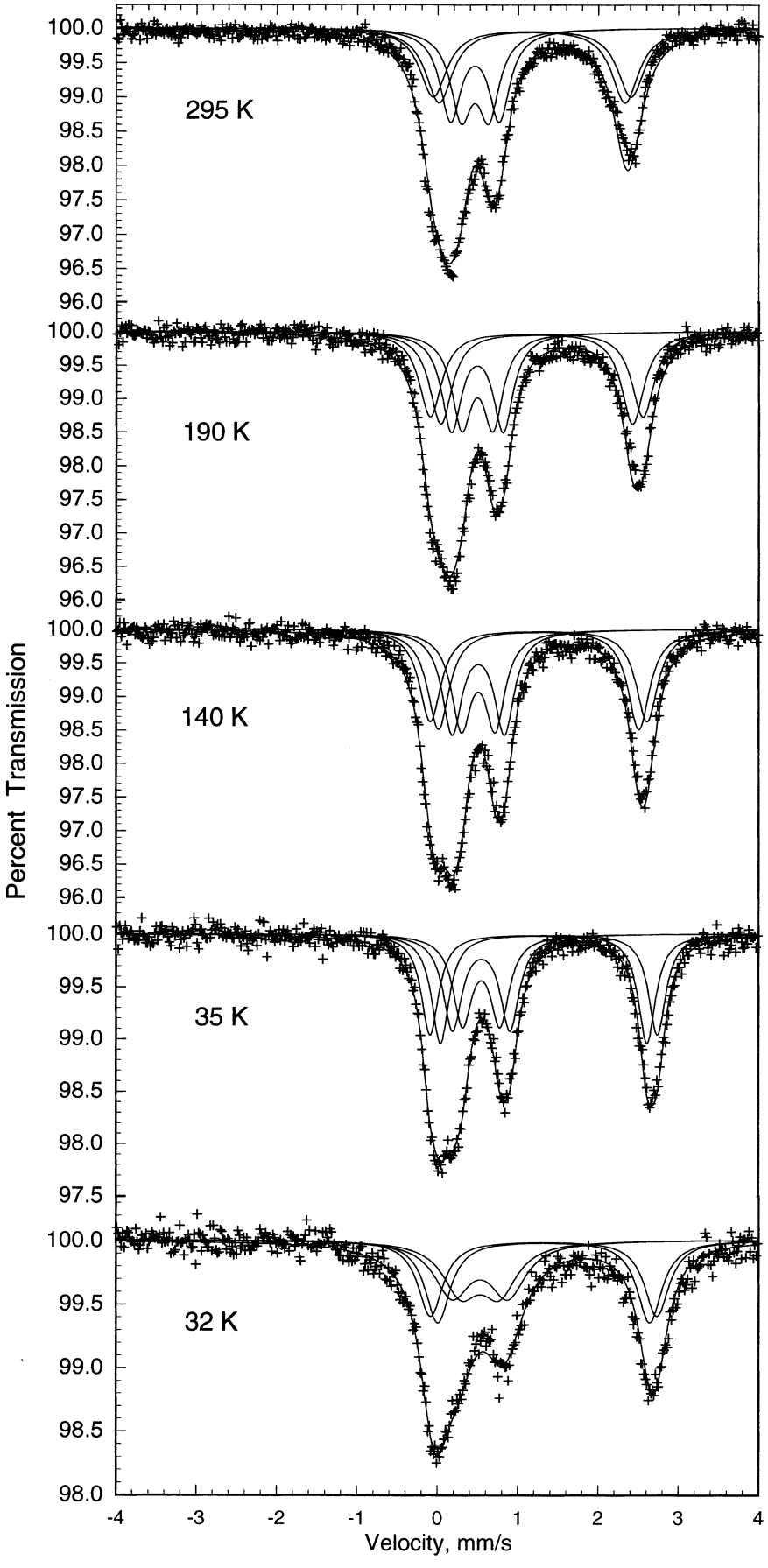

Fig. 8 The temperature dependence of the paramagnetic Mössbauer spectra of synthetic $Na_2MnFe^{II}Fe^{III}(PO_4)_3$ #4

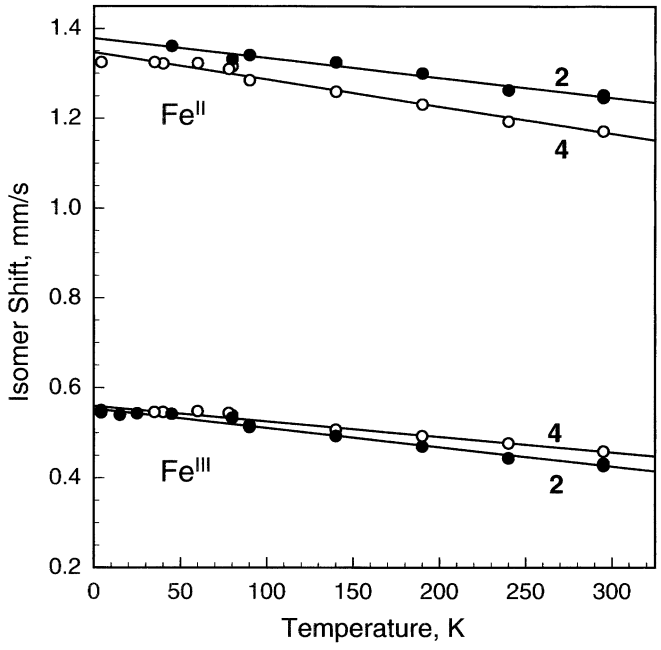

Fig. 9 The temperature dependence of the isomer shifts in NaMn $Fe_2(PO_4)_3$ #2, *closed circles*, and $Na_2MnFe^{II}Fe^{III}(PO_4)_3$ #4, *open circles*. The *error bars* are approximately twice the size of the data points

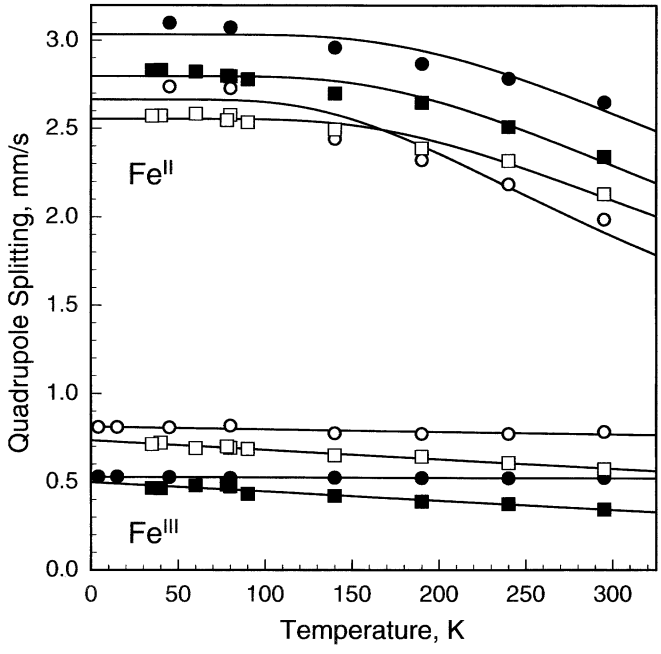

Fig. 10 The temperature dependence of the quadrupole splitting in $NaMnFe_2(PO_4)_3$ #2 *round symbols*, and $Na_2MnFe^{II}Fe^{III}(PO_4)_3$ #4 *square symbols*, where the *closed* and *open symbols* correspond, respectively, to iron ions with an iron(III) or an iron(II) near neighbor on the *M*(2) site. The *error bars* are approximately the size of the data points

observed spectra of #2 and #3 with two iron(III) magnetic sextets with the area ratio expected for the number of iron(III) and iron(II) *M*(2) near neighbors. In all cases, the observed hyperfine fields of ~50 to 54 T (Table 10), are consistent with antiferromagnetically ordered high-spin, $S = 5/2$, iron(III) and, as expected, the iron(III) with an iron(II) *M*(2) near neighbor has a slightly lower hyperfine field. In $Na_2MnFe^{II}Fe^{III}(PO_4)_3$ #4, in addition to the two iron(III) sextets (Fig. 13), two sextets with hyperfine fields of ~24 and 6 T are observed, for the iron(II) ions, ions which have an iron(III) or an iron(II) *M*(2) near neighbor, respectively. The 24 T hyperfine field is typical of antiferromagnetically ordered high-spin, $S = 2$, iron(II) ions and the broad 6 T sextet indicates that the iron(II) with an iron(II) *M*(2) near neighbor is just beginning to show the slow magnetic relaxation associated with its ordering.

It is apparent from the 25 and 30 K spectra shown in Figs. 11 and 12 that magnetic ordering occurs at a higher temperature in synthetic $NaMnFe_2(PO_4)_3$ #2 than in natural $NaMnFe_2(PO_4)_3$ #3. This occurs, no doubt, as a consequence of the traces of Al(III) and Mg(II) found on the *M*(2) site in natural NaMn $Fe_2(PO_4)_3$ #3, diamagnetic cations which are not present in #2, but which reduce the efficacy of the antiferromagnetic exchange ordering and, hence, reduce the Néel antiferromagnetic ordering temperature of #3 relative to that of #2.

Of the four compounds, $Na_2Mn_2Fe(PO_4)_3$ #1 exhibits the lowest iron(III) magnetic hyperfine fields at 4.2 K, fields which are lower because of the presence of manganese(II) on one-half of the near-neighbor *M*(2) sites; but, once again, those iron(III) sites that have an iron(III) *M*(2) near neighbor have a somewhat higher hyperfine field (Table 10) than do those iron(III) sites with a manganese(II) *M*(2) near-neighbor.

Conclusions

Both synthetic and natural iron(III)-containing alluaudite minerals, such as synthetic and natural NaMn $Fe_2(PO_4)_3$ #2 and #3, unexpectedly often have small amounts of iron(II) randomly distributed on the *M*(2) site, iron(II) whose presence somewhat reduces the *M*(2)–*M*(2) cationic interactions and thus stabilizes the alluaudite structure. The presence of some iron(II) on the *M*(2) site has been observed in all the alluaudites we have studied to date (Hermann et al. 2002; Hatert et al. 2003, 2004). Further, the iron(II) *M*(2) site has an ~450 to 600 cm^{-1} low-symmetry component to its pseudooctahedral crystal field. In all cases the manganese(II) is randomly distributed on the *M*(2) site and has relatively little influence on the local electronic symmetry at the iron(II) and/or iron(III) *M*(2) site; it does, however, influence the extent of the antiferromagnetic exchange coupling and, hence, the Néel temperature of the alluaudites. This is revealed by the substantially lower effective magnetic moment and ordering temperature observed for synthetic $Na_2Mn_2Fe(PO_4)_3$ #1, as compared to $NaMnFe_2(PO_4)_3$ #2 and #3 in which one-half

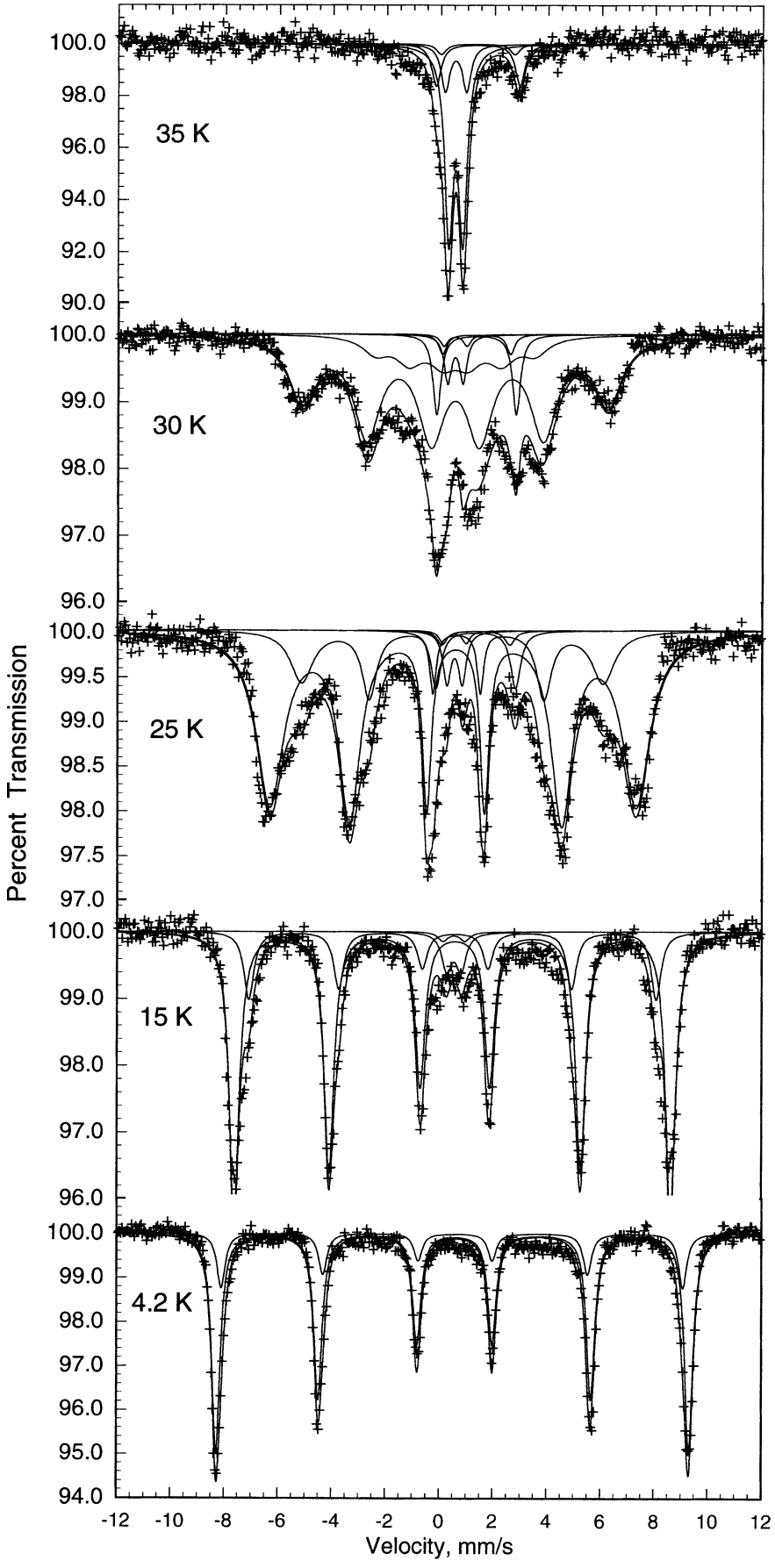

Fig. 11 The temperature dependence of the magnetically ordered Mössbauer spectra of synthetic $NaMnFe_2(PO_4)_3$ #2, obtained at the indicated temperatures

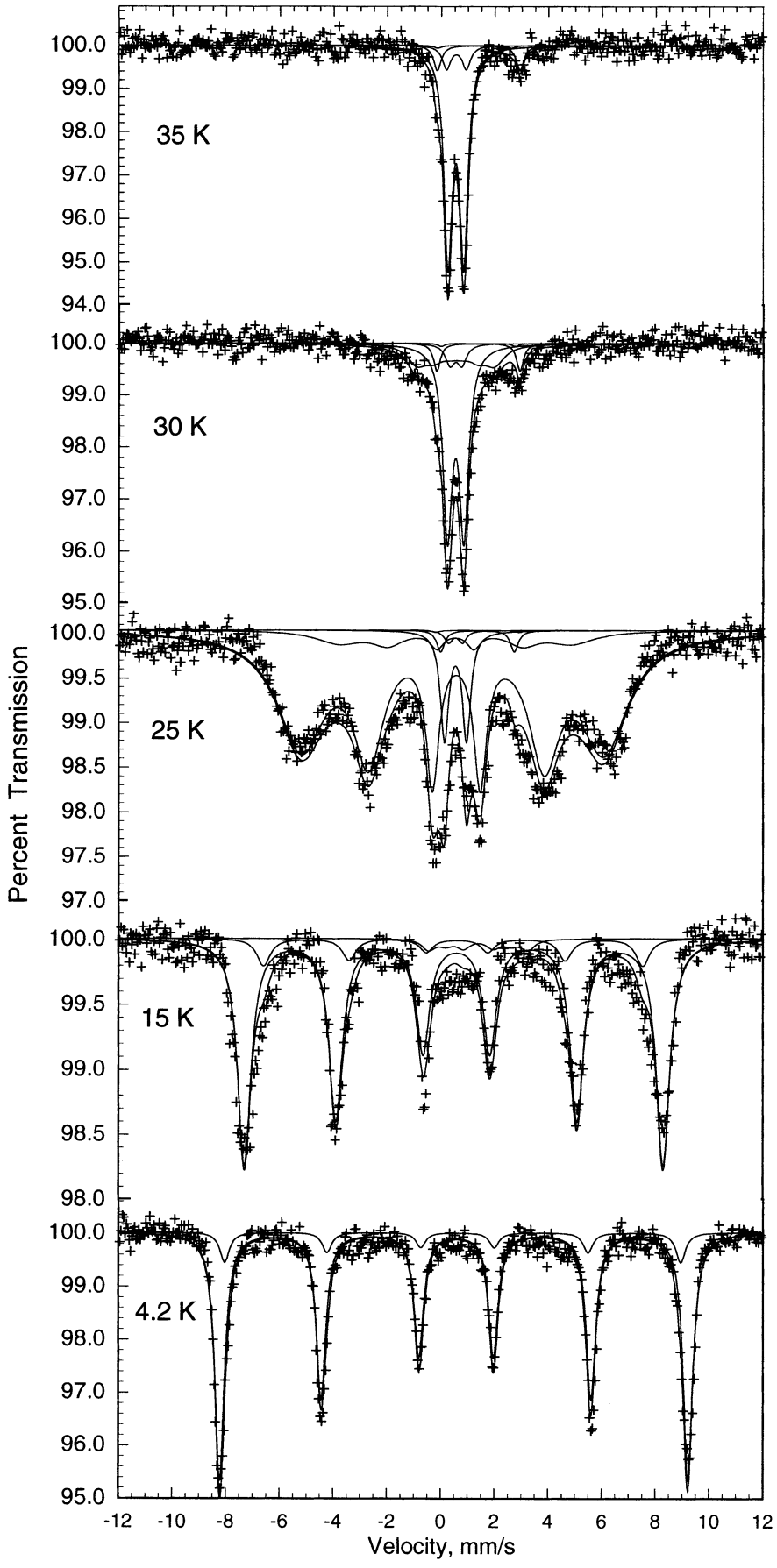

Fig. 12 The temperature dependence of the magnetically ordered Mössbauer spectra of natural $NaMnFe_2(PO_4)_3$ #3, obtained at the indicated temperatures

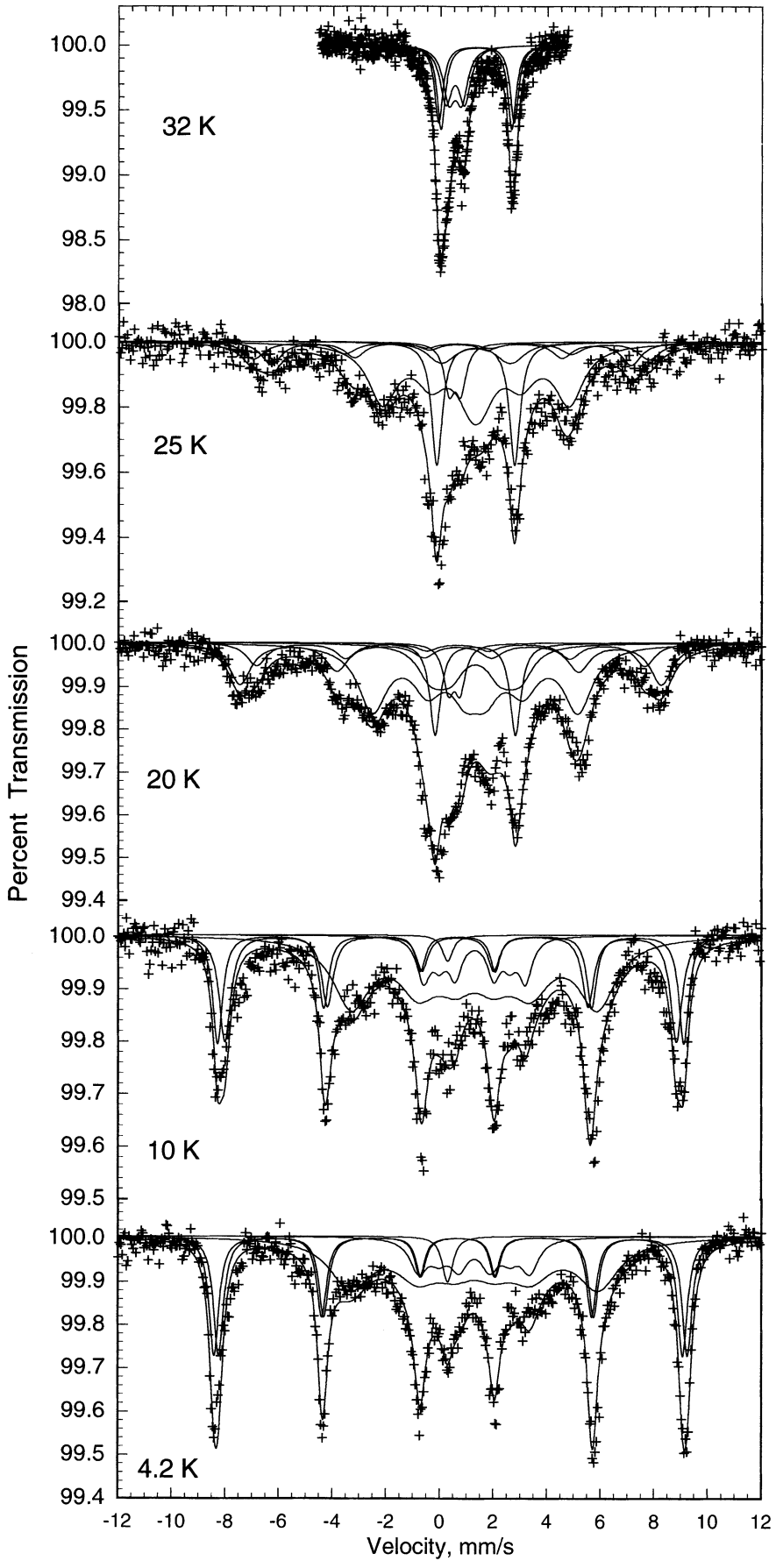

Fig. 13 The temperature dependence of the magnetically ordered Mössbauer spectra of synthetic $Na_2MnFe^{II}Fe^{III}(PO_4)_3$ #4, obtained at the indicated temperatures

Table 10 Selected Mössbauer spectral parameters for antiferromagnetically ordered natural and synthetic alluaudites[a]

Compound	*T*, (K)	$<\delta>$ H, (T)	$<\delta>$ δ, (mm/s^{-1})	ΔE_Q, m (m/s^{-1})	$<\delta>$ Ggr;, (mm/s^{-1})	*Area* %	Assign-ment	*M*(2) near-neighbor
$Na_2Mn_2Fe(PO_4)_3$ #1, Synthetic	4.2	50.4	0.536	−0.92	0.45	50	Fe^{III}	Mn^{II}
		52.2	0.536	−0.61	0.45	50	Fe^{III}	Fe^{III}
$NaMnFe_2(PO_4)_3$ #2, Synthetic	30	18.4	0.540	0.00	1.20	18	Fe^{III}	Fe^{II}
		35.2	0.540	0.00	1.20	70	Fe^{III}	Fe^{III}
	25	34.8	0.540	−0.81	1.00[c]	18	Fe^{III}	Fe^{II}
		42.2	0.540	−0.53	1.22[c]	73	Fe^{III}	Fe^{III}
	15	46.7	0.540	−0.81	0.44	18	Fe^{III}	Fe^{II}
		50.2	0.540	−0.53	0.44	76	Fe^{III}	Fe^{III}
	4.2	53.0	0.545	−0.81	0.37	19	Fe^{III}	Fe^{II}
		54.4	0.545	−0.53	0.37	81	Fe^{III}	Fe^{III}
$NaMnFe_2(PO_4)_3$ #3, Natural	30	9.0	0.539	0.00	0.86	25	Fe^{III}	Fe^{III}
	25	26.8	0.540	−0.85	1.54[c]	9	Fe^{III}	Fe^{II}
		35.0	0.540	−0.58	1.54[c]	82	Fe^{III}	Fe^{III}
	15	43.4	0.540	−0.85	0.60	10	Fe^{III}	Fe^{II}
		48.2	0.540	−0.58	0.60	90	Fe^{III}	Fe^{III}
	4.2	52.3	0.541	−0.85	0.42	10	Fe^{III}	Fe^{II}
		53.9	0.541	−0.58	0.42	90	Fe^{III}	Fe^{III}
$Na_2MnFe_2(PO_4)_3$ #4, Synthetic	25	1.5	1.310	2.57	1.10	7	Fe^{II}	Fe^{II}
		16.0	1.310	2.83	1.30	48	Fe^{II}	Fe^{III}
		41.5	0.530	−0.46	0.90	12	Fe^{III}	Fe^{II}
		45.5	0.530	−0.72	1.00	10	Fe^{III}	Fe^{III}
	20	3.6	1.315	2.57	1.10	15.5	Fe^{II}	Fe^{II}
		18.5	1.315	2.83	1.30	42	Fe^{II}	Fe^{III}
		44.8	0.530	−0.46	0.90	9	Fe^{III}	Fe^{II}
		48.5	0.530	−0.72	1.00	18.5	Fe^{III}	Fe^{III}
	10	5.0	1.295	2.57	0.60	12	Fe^{II}	Fe^{II}
		23.8	1.295	2.83	1.70	47	Fe^{II}	Fe^{III}
		52.1	0.546	−0.46	0.52	22	Fe^{III}	Fe^{II}
		53.7	0.546	−0.72	0.44	18	Fe^{III}	Fe^{III}
	4.2	6.4	1.300	2.57	0.79	13	Fe^{II}	Fe^{II}
		24.1	1.300	2.83	1.86	40	Fe^{II}	Fe^{III}
		53.5	0.546	−0.46	0.44	22.5	Fe^{III}	Fe^{II}
		54.5	0.546	−0.72	0.44	22.5	Fe^{III}	Fe^{III}

[a] The paramagnetic components have not been included in this table and as a result the spectral areas do not in all cases sum to 100%

[b] The isomer shifts are given relative to room temperature α-iron foil.

[c]The line width of the outer line of the magnetic sextet

of the manganese(II) has been replaced. All of the alluaudites studied herein are antiferromagnetically ordered as a result of magnetic exchange coupling along the staggered chains containing the *M*(2) cation pairs, an exchange which is mediated by the manganese(II) on the *M*(1) site. Further, it should be noted that the presence of manganese(II) on the *M*(2) site in $Na_2Mn_2Fe(PO_4)_3$ #1 increases this magnetic exchange coupling and, as a consequence #1 has a somewhat higher ordering temperature of 40 K as compared to the 35, 32, and 35 K ordering temperatures of #2–4, respectively.

Acknowledgements Gary J. Long thanks the Francqui Foundation of Belgium for his appointment as a Chaire Francqui Interuniversitaire au titre étranger during the 2002–2003 academic year. The authors also acknowledge with thanks the financial support of the US National Science Foundation through grant DMR-95–21739 and the Fonds National de la Recherche Scientifique, Belgium, through grant 9.456595, and the Fonds de la Recherche Fondamentale Collective, Belgium, through grants 2.4531.00F and 2.4522.01. Marie-Jeanne Hubin-Franskin and Frédéric Hatert acknowledge support from the Fonds National de la Recherche Scientifique, Belgium, as a Directeur de Recherches and a Chargé de Recherches, respectively.

References

Antenucci D, Miehe G, Tarte P, Schmahl WW, Fransolet A-M (1993) Combined X-ray Rietveld infrared and Raman study of a new synthetic variety of alluaudite, $NaCdIn_2(PO_4)_3$. Eur J Mineral 5: 207–213

Burnham CW (1991) LCLSQ version 8.4, least-squares refinement of crystallographic lattice parameters. Dept Earth and Planetary Sciences, Harvard University

Chouaibi N, Daidouh A, Pico C, Santrich A, Veiga ML (2001) Neutron diffraction, Mössbauer spectrum, and magnetic behavior of $Ag_2FeMn_2(PO_4)_3$ with an alluaudite-like structure. J Solid State Chem 159: 46–50

Daidouh A, Durio C, Pico C, Veiga ML, Chouaibi N, Ouassini, A (2002) Structural and electrical study of the alluaudites $(Ag_{1-x}Na_x)_2FeMn_2(PO_4)_3$ (x = 0, 0.5 and 1). Solid State Sci 4: 541–548

Durio C, Daidouh A, Chouaibi N, Pico C, Veiga ML (2002) Electrical behavior of new orthophosphates $Na_2M_3(PO_4)_3$ (M_3 = $GaMn_2$, $GaCd_2$, $InMn_2$ and FeMnCd) with the alluaudite-like structure. J Solid State Chem 168: 208–216

Fisher DJ (1955) Alluaudite. Am. Mineral. 40: 1100–1109

Fransolet A-M (1975) Etude minéralogique et pétrologique des phosphates des pegmatiques granitiques. Doctoral thesis, University of Liège, 333 pp

Goodenough JB (1963) Magnetism and the chemical bond. Wiley-Interscience, New York, pp 180–183

Hatert F (2002) Cristallochimie et synthèse hydrothermale d'alluaudites dans le système Na–Mn–Fe–P–O: contribution au problème de la genèse de ces phosphates dans les pegmatites granitiques. Doctoral thesis, University of Liège, 247 pp

Hatert F, Keller P, Lissner F, Antenucci D, Fransolet A-M (2000) First experimental evidence of alluaudite-like phosphates with high Li content: the $(Na_{1-x}Li_x)MnFe_2(PO_4)_3$ series ($x = 0$ to 1). Eur J Mineral 12: 847–857

Hatert F, Hermann RP, Long GJ, Fransolet A-M, Grandjean F (2003) An X-ray Rietveld, infrared, and Mössbauer spectral study of the $NaMn(Fe_{1-x}In_x)_2(PO_4)_3$ alluaudite-type solid solution. Am Mineral 88: 211–222

Hatert F, Rebbouh L, Hermann RP, Fransolet A-M, Long GJ, Grandjean F (2004) Hydrothermal synthesis and crystal chemistry of the $Na_2(Mn_{1-x}Fe^{2+}{}_x)_2Fe^{3+}(PO_4)_3$ alluaudite-type solid solution. Am. Mineral. Submitted for publication.

Hermann RP, Hatert F, Fransolet A-M, Long GJ, Grandjean F (2002) Mössbauer spectral evidence for next-nearest neighbor interactions within the alluaudite structure of the $Na_{1-x}Lin_xMnFe_2(PO_4)_3$. Solid State Sci 4: 507–513

Ingalls R (1964) Electric-field gradient tensor in ferrous compounds. Phys Rev 133A: 787–A795

Korzenski MB, Schimek GL, Kolis JW, Long GJ (1998) Hydrothermal synthesis, structure, and characterization of a mixed-valent iron(II/III) phosphate, $NaFe_{3.67}(PO_4)_3$: a new variation of the alluaudite structure type. J Solid State Chem 139: 152–160

Long GJ, Baker Jr WA (1971) On the magnetic properties of some distorted octahedral high-spin iron(II) complexes. J Chem Soc (A) 2956

Moore PB (1971) Crystal chemistry of the alluaudite structure type: Contribution to the paragenesis of pegmatite phosphate giant crystals. Am Mineral 56: 1955–1975

Moore PB, Ito J (1979) Alluaudites, wyllieites, arrojadites: crystal chemistry and nomenclature. Min Mag 43: 227–235

Richardson TJ (2003) Phosphate-stabilized lithium intercalation compounds. J Power Sources 119–121: 262–265

Renner B, Lehmann, G (1986) Correlation of angular and bond length distortion in TiO_4 units in crystals. Z Kristallogen 175: 43–59

Shannon RD (1976) Revised effective ionic radii and systematic studies of interatomic distances in halides and chalcogenides. Acta Crystallogen A32: 751–767

Tuttle OF (1949) Two pressure vessels for silicate-water studies. Geol Soc Am Bull 60: 1727–1729

Ungethüm H (1965) Eine neue Methode zur Bestimmung von Eisen(II) in Gesteinen und Mineralen, insbesondere auch in bitumenhaltigen Proben. Z angew Geol. 11: 500–505

Varret F, Czeskleba H, Hartmann-Boutron F, Imbert P (1972) Etude par effet Mössbauer de l'ion Fe^{2+} en symétrie trigonale dans les composés du type $(Fe,M)_2Mo_3O_8$ (M = Mg, Zn, Mn, Co, Ni) et propriétés magnétiques de $(Fe,Zn)_2Mo_3O_8$. J Phys 33: 549–564

Warner TE, Milius W, Maier J (1994) New copper phosphates with the NASICON or alluaudite-type structures as ionic or mixed conductors. Solid State Ionics 74: 119–123

Young RA, Larson AC, Paiva-Santos CO (1998) User's guide to program DBWS-9807 for Rietveld analysis of X-ray and neutron powder diffraction patterns. School of Physics, Georgia Institute of Technology, Atlanta, USA, 56 pp